ATMOSPHERIC DENSITY ESTIMATION USING SATELLITE PRECISION ORBIT EPHEMERIDES

BY

Anoop Kumar Arudra

Submitted to the graduate degree program in Aerospace Engineering and the Graduate Faculty of the University of Kansas in partial fulfillment of the requirements for the degree of Master of Science

Chairperson: Dr. Craig McLaughlin

Committee members

Dr. Ray Taghavi

Dr. Shahriar Keshmiri

Date defended: 11 April, 2011

The Thesis Committee for Anoop Kumar Arudra certifies that this is the approved Version of the following thesis:

ATMOSPHERIC DENSITY ESTIMATION USING SATELLITE PRECISION ORBIT EPHEMERIDES

Committee:

Chairperson: Dr. Craig McLaughlin

Dr. Ray Taghavi

Dr. Shahriar Keshmiri

Date approved: 11 April, 2011

ABSTRACT

The current atmospheric density models are not capable enough to accurately model the atmospheric density, which varies continuously in the upper atmosphere mainly due to the changes in solar and geomagnetic activity. Inaccurate atmospheric modeling results in erroneous density values that are not accurate enough to calculate the drag estimates acting on a satellite, thus leading to errors in the prediction of satellite orbits. This research utilized precision orbit ephemerides (POE) data from satellites in an orbit determination process to make corrections to existing atmospheric models, thus resulting in improved density estimates.

The work done in this research made corrections to the Jacchia family atmospheric models and Mass Spectrometer Incoherent Scatter (MSIS) family atmospheric models using POE data from the Ice, Cloud and Land Elevation Satellite (ICESat) and the Terra Synthetic Aperture Radar – X Band (TerraSAR-X) satellite. The POE data obtained from these satellites was used in an orbit determination scheme which performs a sequential filter/smoother process to the measurements and generates corrections to the atmospheric models to estimate density. This research considered several days from the year 2001 to 2008 encompassing all levels of solar and geomagnetic activity. Density and ballistic coefficient half-lives with values of 1.8, 18, and 180 minutes were used in this research to observe the effect of these half-life combinations on density estimates. This research also examined the consistency of densities derived from the accelerometers of the Challenging Mini Satellite

Payload (CHAMP) and Gravity Recovery and Climate Experiment (GRACE) satellites by Eric Sutton, from the University of Colorado. The accelerometer densities derived by Sutton were compared with those derived by Sean Bruinsma from CNES, Department of Terrestrial and Planetary Geodesy, France. The Sutton densities proved to be nearly identical to the Bruinsma densities for all the cases considered in this research, thus suggesting that Sutton densities can be used as a substitute for Bruinsma densities in validating the POE density estimates for future work.

Density estimates were found using the ICESat and TerraSAR-X POE data by generating corrections to the CIRA-72 and NRLMSISE-00 atmospheric density models. The ICESat and TerraSAR-X POE density estimates obtained were examined and studied by comparing them with the density estimates obtained using CHAMP and GRACE POE data. The trends in how POE density estimates varied for all four satellites were found to be the same or similar. The comparisons were made for different baseline atmospheric density models, different density and ballistic coefficient correlated half-lives, and for varying levels of solar and geomagnetic activity. The comparisons in this research help in understanding the variation of density estimates for various satellites with different altitudes and orbits.

ACKNOWLEDGEMENTS

With great pleasure I would like to express my sincere gratitude to Dr. Craig McLaughlin, my advisor and committee chair, for giving me the opportunity to perform this research. I am very much thankful to him for his invaluable guidance, help, and advice throughout the course of this research work. I would also like to thank Dr. Shahriar Keshmiri and Dr. Ray Taghavi for agreeing to be my committee members.

I would also like to thank Andrew Hiatt and Travis Lechtenberg, whose earlier work contributed a lot in completing my research work. I would like to thank my group members Eric Fattig and Dhaval Mysore for their help in answering my questions throughout this research work.

Lastly, I should take this opportunity to express my special regards to my parents, my sister, and my friends for their love, support and encouragement throughout my education.

TABLE OF CONTENTS

NOMENCLATURE

Symbol	Definition	Units
a_D	acceleration vector due to atmospheric drag	m/s^2
a_p	geomagnetic 3-hourly planetary equivalent amplitude index	gamma, Tesla, or kg s m^{-1}
A	satellite cross-sectional area	m^2
A_p	geomagnetic daily planetary amplitude index	gamma, Tesla, or kg s m^{-1}
$\Delta B/B$	estimated ballistic coefficient correction	~
BC	Inverse ballistic coefficient	m^2/kg
c_D	satellite drag coefficient	~
d	cross correlation delay	
$F_{10.7}$	daily solar radio flux measured at 10.7 cm wavelength	SFU
g_o	gravitational acceleration	m/s^2
Δh	altitude change	m
i	cross correlation series index	
j	user defined Gauss-Markov correlated half-life time series index	
k	Gauss-Markov sequence index	
K_p	geomagnetic planetary index	~
m	satellite mass	kg

mx	mean of series x	
my	mean of series y	
M	mean molecular mass	amu
N	number of elements	
r	cross correlation coefficient	
R	universal gas constant	$J\ K^{-1}\ mol^{-1}$
t	time	S
T	temperature	K
v_{rel}	satellite velocity magnitude relative to Earth's atmosphere	m/s
$w(t)$	Gaussian white random variable	
x	x component of satellite position vector	m
x	Gauss-Markov process dynamic scalar random variable	
x	cross correlation series	
$\boldsymbol{X}$	satellite state vector	
y	y component of satellite position vector	m
y	cross correlation series	
z	z component of satellite position vector	m

Greek Letters	**Definition**	**Units**

α	Gauss-Markov process variable	
$\Delta\rho/\rho$	estimated atmospheric density correction	~
ρ	atmospheric density	kg/m^3
σ_w^2	variance of Gaussian white random variable	
τ	user defined correlated half-life	
ω_{Earth}	Earth's angular velocity magnitude	rad/s
Φ	transition function	

Abbreviations	**Definition**
CHAMP	Challenging Minisatellite Payload
CIRA	COSPAR International Reference Atmosphere
COSPAR	Committee on Space Research
CNES	Centre National d'Études Spatiales
DCA	Dynamic Calibration of the Atmosphere
DTM	Drag Temperature Model
EUV	Extreme Ultra-Violet
GPS	Global Positioning System
GRACE	Gravity Recovery And Climate Experiment
GSFC	Goddard Space Flight Center
HASDM	High Accuracy Satellite Drag Model
ICESat	Ice, Cloud, and Land Elevation Satellite

MSISE	Mass Spectrometer Incoherent Scatter Extending from ground to space
NASA	National Aeronautics and Space Administration
NORAD	North American Aerospace Defense Command
NRLMSISE	Naval Research Laboratory Mass Spectrometer Incoherent Scatter Extending from ground to space
ODTK	Orbit Determination Tool Kit
POE	Precision Orbit Ephemerides
PSO	Precision Science Orbit
RSO	Rapid Science Orbit
SETA	Satellite Electrostatic Triaxial Accelerometer
SFU	Solar Flux Units
SLR	Satellite Laser Ranging
STAR	Spatial Triaxial Accelerometer for Research
TLE	Two Line Element
TerraSAR-X	Terra Synthetic Aperture Radar- XBand

LIST OF FIGURES

LIST OF TABLES

1. INTRODUCTION

1.1 Objective

The main objective of this research is to make corrections to a given atmospheric density model using satellite precision orbit ephemerides (POE) in an orbit determination technique and estimate accurate density values. The resulting estimated density values help in achieving better drag estimates on the satellites leading to more accurate prediction and determination of the satellite orbit.

1.2 Motivation

The motivation for this research arises from the need to achieve more precise orbit determination than the orbits predicted using density values obtained from current atmospheric density models. Current atmospheric models account for only the variations occurring for longer time periods in the atmosphere and yield density values which are not accurate enough for the better prediction of satellite orbits. This research focuses on shorter periods of atmospheric density variations for better density estimates.

In low Earth orbit (LEO), where most satellites orbit, the variation of the atmospheric density is very high and the actual density values may differ widely from the values predicted by current atmospheric density models. These rapid changes in the variations are not accurately accounted for by the present atmospheric models and can affect the prediction of satellite orbits. Therefore, accurate density

calculations are required for better atmospheric drag estimates, which result in better orbit predictions.

The Earth's upper atmosphere is mostly influenced by solar and geomagnetic activity. Fluctuating intensities of solar radiation and Earth's magnetic field are responsible for variations of atmospheric density. Primarily, the Sun heats up the Earth's atmosphere through EUV radiation. In addition, charged particles from the Sun interact with the Earth's magnetic field resulting in geomagnetic activity. The current atmospheric models use the solar flux data and Earth's magnetic field data as daily or three hour averaged values as inputs for estimating density. These daily or three hour time periods are too large and cannot result in better orbit determination. Smaller time scales are preferable over these daily or three hour periods for improvements in orbit determination, Ref. [1].

To achieve more accurate orbit determination and prediction, corrections are required for the current atmospheric density models. In this research corrections are made to the atmospheric models utilizing satellite precision orbit ephemerides (POE) data in a precision orbit determination technique. As a result, more accurate densities are obtained by generating corrections to the atmospheric models. For this research, the POE data of four different satellites, Challenging Minisatellite Payload (CHAMP); Gravity Recovery and Climate Experiment (GRACE); Ice, Cloud, and Land Elevation Satellite (ICESat); and Terra Synthetic Aperture Radar, X-band satellite (TerraSAR-X) were used.

The improved density estimates obtained can be used to calculate better atmospheric drag estimates by using them in the drag equation. Increased accuracy in density estimates results in better drag estimates which in turn improves the determination and prediction of satellite orbits. It also helps in estimating a satellite's lifetime and its time of reentry. Also, better density estimates from the corrected atmospheric models paves the way for understanding the effects of the space environment and space weather in Earth's atmosphere.

1.3 Atmospheric Density

This research primarily deals with the correcting of atmospheric density models and generating atmospheric density estimates. So a brief introduction to the neutral atmosphere and its structure and factors contributing to the variation of atmospheric density is given in the subsequent sections. References 1-5 contribute most of the information discussed in this section and its subsections.

1.3.1 Neutral Atmosphere

The atmosphere of the earth consists of different types of gas molecules including carbon dioxide, oxygen, nitrogen, argon, ozone, hydrogen, and helium in varying proportions. The presence of these gas molecules in varying proportions across the atmosphere results in the variation of density of the atmosphere. As the altitude increases, the atmospheric density gradually decreases due to hydrostatic equilibrium. Earth's atmosphere absorbs energy from the sun and as the altitude increases the intensity of UV radiation from the Sun increases resulting in the

disassociation of these gas molecules. The temperature T, pressure P, and density ρ of atmosphere are connected by the well known gas law [Ref. 1]

$$\rho = \frac{pM}{RT} \qquad (1.1)$$

Where, R is the gas constant (8.31 J/K.mol) and M is the molecular weight of the gas.

The decrease of pressure with height h is given by the hydrostatic equation [Ref. 1]

$$\frac{dp}{dh} = -\rho g\,, \qquad (1.2)$$

Where, g is the acceleration due to gravity.

1.3.2 Layers of the Atmosphere

The information contained in this subsection is summarized from Ref [1]. All the altitude and temperature values mentioned in this section are only average values. Depending upon the temperature variation, the atmosphere is classified into five different layers namely, the troposphere, stratosphere, mesosphere, thermosphere, and exosphere where the boundary of each layer is separated from the next by transition regions called the tropopause, stratopause, mesopause, and thermopause which extend over a very small altitude and have nearly constant temperature.

The troposphere is the densest layer of the atmosphere and extends to an altitude of 0-12 km. In the troposphere the temperature drops as altitude increases

from 293K to 233K approximately at a rate of 6.5K km^{-1}, known as the lapse rate. The next layer is the stratosphere which extends from 12- 50 km in altitude. This is a less dense layer when compared to the troposphere and contains an ozone layer at an altitude of 20-30 km which absorbs the UV radiation resulting in the increase of temperature from 223K to 270K as the altitude increases. The next layer is the mesosphere with an altitude range of 50-85 km. The temperature decreases from 270K to 180-200K at its upper boundary. The molecules in the mesosphere are in an active state from the energy absorbed from the Sun. The next layer after the mesosphere is the thermosphere which extends from 85-600 km in altitude. Here the temperature increases considerably from 180-200K to 1000-1800K. The thermosphere is much less dense so that a small change in solar activity causes a significantly large change in the temperature. The predominant gas molecule here is atomic oxygen. The final layer of the atmosphere is the exosphere with an altitude range of 600 – 10,000 km which extends into interplanetary space. The major components of the exosphere are hydrogen and helium with low densities and some atomic oxygen near the bottom of the exosphere. The gases from the exosphere can escape into space. [Ref. 1]

The thermosphere and exosphere are the two important layers to be considered for the problem of orbit determination and the disturbances from the other three lower levels propagating into thermosphere and exosphere are of less interest. Satellites orbiting in LEO are of great concern for orbit determination problems as they experience the most drag because of the higher density in the thermosphere and

lower exosphere. LEO lies at an altitude of 100km -1000km within the regions of the thermosphere and exosphere. The ambient neutral atmosphere is an important environment in LEO. In the neutral atmosphere, the electrically neutral particles in the atmosphere interact both mechanically (aerodynamic drag/physical sputtering) and chemically (atomic oxygen attack/spacecraft glow) with satellites. [Ref. 1]

1. 3.3 Variations in Atmospheric Density

Generally the values of three basic neutral atmospheric parameters, density, temperature, and composition, vary in response to many factors such as local time, latitude, longitude, altitude, solar and geomagnetic activity. Solar and geomagnetic activities contribute to the sudden large scale fluctuations in the atmosphere. Short term density fluctuations affect orbital position, complicating tracking and satellite communication. Long term changes can dominate satellite lifetime. The density variations can be estimated from atmospheric models. Most important in assessing the effect of air drag on orbits are the variations in air density, namely the form of its variation with height, time between day and night, and above all the dependence of density on solar activity. [Ref. 2]

Some of the phenomena that are responsible for the long term and short term variations of the neutral atmospheric density are discussed in the following subsections.

1.3.3.1 Solar Cycles

The Sun has a great influence on the space environment. Several hundred years of observations of the Sun revealed a changing pattern of disturbances that appear to follow semi-regular patterns of about 11 years called solar cycles. These solar cycles are somewhat predictable in time and have peak activity levels. These solar cycles cause long term variations in the neutral atmosphere due to an increase in extreme ultraviolet radiation (EUV) flux from the Sun and an increase in geomagnetic activity related to variations in the solar wind. As solar activity increases, the temperature in the atmosphere rises resulting in an increase of the density of the atmosphere. [Ref. 2]

1.3.3.2 Solar Flares

The Sun is constantly changing. Visual confirmation of this change is often seen in the form of solar flares. A flare is the sudden brightening of the chromosphere. Solar flares sometimes create energetic particle events in LEO and these particles couple with the changes in EUV flux that heat the atmosphere. This occurs far more frequently during solar maxima than solar minima and lasts from few minutes to a few hours. [Ref. 2]

1.3.3.3 27 Day Solar Rotation Cycle

This effect comes from the Sun's rotational period of 27 days and causes a fluctuation in the atmosphere. An active region of the Sun will return approximately every 27 days. [Ref. 2]

1.3.3.4 Geomagnetic Storms and Substorms

The boundary between the region where the Sun's magnetic field dominates and where the Earth's magnetic field dominates is called the magnetopause. The Sun's magnetic field fluctuates in response to solar phenomena. Consequently the magnetopause moves in response to the Sun's field. These fluctuations are called magnetic storms and are typically quite small. Variation in the solar wind is the primary energy source for these events. These geomagnetic storms often follow a sudden change in geomagnetic field and can last for several days. [Ref. 2]

1.3.3.5 Diurnal Variations

Diurnal Variations occur every day as Earth rotates. Day to night density variation occurs because of the temperature variation from day to night. The density has a minimum at about 4 a.m and a maximum at about 2 p.m, local time. This variation occurs regularly each day with maximum density being about 5 times greater than the minimum density. [Ref. 2]

1.3.3.6 Semiannual / Seasonal Variations

There are also seasonal effects on the atmosphere because of differential heating as the angle of incidence of the Sun changes. Solar activity and tides cause large diurnal and semidiurnal global density variations. In a normal year the density has maxima during April and in late October and minima during January and July.

These last up to 6 months and are related to varying distance of the Earth from the Sun and the Sun's declination during the year. [Ref. 2]

1.3.3.7 Gravity Waves and Thermospheric Winds

Gravity waves in the atmosphere are small scale spatial density and temperature fluctuations of approximately 100 km in dimension. They are driven by a number of sources including auroral particle fluxes, thunderstorms and mountain ranges. High latitude thermospheric winds with velocities up to 1 km/sec have been observed, which can cause drag induced errors in satellite orbits. [Ref. 2]

1.3.3.8 Latitudinal and Longitudinal Variations

Latitudinal variations are easiest to visualize. Passing over the Earth's equatorial bulge effectively changes the actual altitude and density, which in turn changes the drag. Change in longitude changes altitude because of mountain ranges and oceans, and causes changes in wind direction, and differences in density and temperature. [Ref. 2]

1.3.4 Solar and Geomagnetic Indices

The density of upper atmosphere changes mainly due to solar flux and geomagnetic activity. Solar flux affects atmospheric density through instantaneous heating from EUV. Geomagnetic activity affects the atmosphere through delayed heating of atmospheric particles from collisions with charged energetic particles from the Sun.

1.3.4.1 Solar Flux Data

An important indicator or measure of solar activity is the $F_{10.7}$ flux. It is the solar radio flux observed at a wavelength of 10.7 cm by the National Research Council since 1947. It corresponds to a radio emission line for iron and is normally reported in solar flux units (SFU). 1 SFU = 10^{-22} $Wm^{-2}Hz^{-1}$, [Ref.3]. Variations of $F_{10.7}$ are believed to correlate with variations of the solar EUV flux and are correlated with the long term variations in solar activity. $F_{10.7}$ varies from about 50 SFU at solar minima to 240 SFU at solar maxima and varies with the 11 year solar cycle.

Solar Activity depending on the $F_{10.7}$ SFU data is classified as follows, [Ref. 7]:

Solar Activity	Solar Flux ($F_{10.7}$)
Low	$F_{10.7}$ <75
Moderate	75< $F_{10.7}$ <150
Elevated	150< $F_{10.7}$ <190
High	190< $F_{10.7}$

Table 1.1 Solar Activity Bin [Ref. 7]

1.3.4.2 Geomagnetic Activity Index

The short term geomagnetic activity accounted for every 3 hours are given as semi-logarithmic (K_p) values or in its linearized form (a_p). These indices represent magnetic field disturbances induced by changes in the solar wind and through heating effects and are correlated with the short term variations of the upper atmosphere. The subscript p refers to planetary because the indices are the result of combining values from individual stations around the world. Although the K_p index is

the most fundamental quantity, its linearized version a_p is more easily understood. The a_p values are selected so that they correspond to the maximum variations in the Earth's surface magnetic field at mid latitudes in a 3 hr period. The a_p and its daily average A_p range from a minimum value of zero to a maximum value of 400. [Ref. 3]

Geomagnetic activity depending on the level of A_p index is categorized as follows, [Ref. 8]:

Geomagnetic Activity	Daily Planetary Amplitude (A_p)
Quiet	$A_p<10$
Moderate	$10<A_p<50$
Active	$50<A_p$

Table 1.2 Geomagnetic Activity Bin [Ref. 8]

1.4 Effect of Atmospheric Drag on Satellites

Satellites in Earth orbit are subjected to various perturbations like the oblateness of the Earth, air drag, luni-solar forces of attraction, and solar radiation pressure. Of all these perturbations, atmospheric drag acting on satellites is the most important effect for low LEO. The study of drag is to determine orbits under the influence of drag, estimate a satellite's lifetime, and determine the physical properties of the atmosphere. Atmospheric drag on low Earth orbiting satellites is the key parameter in predicting a satellite's lifetime and orbital parameters

1.4.1 Drag Equation

Density is the most important atmospheric parameter which directly controls the air drag felt by satellites passing through the upper atmosphere. Density can be determined by measuring the drag on satellites. The neutral atmosphere in LEO exerts an aerodynamic drag force on the satellite due to the impact of atmospheric particles on the satellite surface. When the gas molecules of the neutral atmosphere in LEO impact a satellite, they transfer energy and momentum to the satellite. The satellite will feel this exchange of momentum as a drag force.

The drag force on the satellite is a force anti-parallel or opposite the velocity vector which is given by the drag equation as [5]

$$D = -\tfrac{1}{2} C_d \rho v^2 A \qquad (1.3)$$

Where D is the drag force, ρ is the ambient atmospheric neutral density, A is the cross sectional area of the satellite projected onto the velocity vector, v is the satellite velocity relative to the atmosphere, and C_d is the drag coefficient that represents how much drag deviates from the momentum flux in the ambient free stream [Ref. 5]. The drag equation can also be written as

$$a_D = -\frac{1}{2} \rho v^2 \frac{C_d A}{m} \qquad (1.4)$$

Where a_D is the acceleration due to drag and m is the mass of the satellite. An important parameter in the above equation is the ballistic coefficient, BC $= \frac{m}{C_d A}$. It is a measure of a satellite's susceptibility to drag effects. A low BC means drag will affect a satellite more and vice versa. But in this research we use the inverse ballistic coefficient, B$= \frac{C_d\ A}{m}$, because the values should be consistent with the usage in Orbit Determination Tool Kit (ODTK) software used in this research. With this new relationship, a lower B means a lower drag effect on the satellite. [Ref. 2]

1.4.2 Satellite Parameters

Atmospheric density and a satellite's BC play crucial roles in accurately determining drag. Determining atmospheric density is a very difficult part of the process. But the problems with determining a satellite's BC may not be so apparent. These calculations involve the cross sectional area, drag coefficient, and satellite mass. [Ref. 5]

1.4.2.1 Drag coefficient

There is no exact value for the drag coefficient C_d. For a satellite in orbit at a height of 200-300 km, the drag coefficient is usually taken as 2.2 for a spherical shape and at heights near 800 km at solar minimum with helium as the chief constituent C_d is taken as 2.5. But when a standard value is needed for C_d, 2.2 is adopted which is appropriate for a sphere or rotating cylinder or rotating convex

bodies. For concave bodies, it is difficult to calculate C_d and detailed geometric analysis is required, [Ref. 5]. Slight changes in drag coefficient greatly change the result, which is why an effective drag coefficient is usually estimated in orbit determination. [Ref. 5]

1.4.2.2 Area

Cross-sectional area is defined to be the area which is normal to the velocity vector. Evaluating the cross-sectional area of a spherical satellite is simple, but for other shapes it is more difficult. If the satellite is attitude controlled the cross section can be calculated, though often with difficulty, if size, shape, and attitude are known. The satellite cross-sectional area is determined by the configuration and orientation of the satellite. This cross-section can vary because it is determined by the presence of large solar arrays or antennas. [Ref. 5]

1.4.2.3 Velocity

The velocity of a satellite relative to the atmosphere is expressed in terms of v_{rel}, the orbital velocity relative to Earth's center and the velocity of air relative to the Earth's center, v_{atm}. The vector velocity v_{rel} of the satellite relative to the Earth's center is the vector sum of satellite velocity v_{sat} relative to the air and velocity v_{atm} of the air relative to Earth's center. The velocity equation is given as [5]

$$v_{sat} = v_{rel} - v_{atm} \tag{1.5}$$

1.4.2.4 Mass and Ballistic Coefficient

The mass of the satellite is given by the manufacturing company. In the course of time, the mass of the satellite changes due to maneuvers. For most satellites finding area and coefficient of drag accurately is a difficult process. Therefore, it is common to use ballistic coefficient, BC in the equation, which incorporates mass, area and C_d, [Ref.6]. In this research the BC of a satellite is estimated as corrections to a nominal value.

1.4.3 Effects of Drag

The general effect of atmospheric drag on the evolution of the orbit of a satellite is the contraction of the apogee altitude. During each orbit, the spacecraft spends increasingly more time at perigee because of higher atmospheric densities until drag becomes so large that the orbit very quickly degenerates and the spacecraft reenters the atmosphere. The drag may not be strictly in the tangential direction to the orbit because atmospheric winds and rotation of the atmosphere will exert small lateral forces on the trajectory. The ability to precisely determine the orbit of a spacecraft is a sensitive function of atmospheric drag. Air drag is responsible for ending a satellite's life by changing or reducing the semi major axis, a, and eccentricity of the orbit, e. [Ref. 4]

1.5 Atmospheric Density Models

Accurately modeling the atmosphere is difficult because knowledge of the physical properties of the atmosphere is very limited. However, several atmospheric models were developed over several years based on assumptions about atmospheric drag, solar and geomagnetic indices, and some other related parameters. These atmospheric models describe the variation of different gas properties in the atmosphere as a function of altitude. We need a good enough model to account for the atmospheric density while accurately modeling the effects of drag on an orbit. Different models are required for different applications. There are several models that can be used to estimate atmospheric density and constituents as a function of altitude, latitude, longitude, year, day, and time. Some of the important and familiar models from the oldest Jacchia family of models to the recent NRLMSIS model are explained in brief below.

1.5.1 Jacchia 1971

Different atmospheric density models have been published by L.G Jacchia (1965, 1970, 1971, and 1977). The first model was J65 which is entirely based upon the primary parameters, geodetic height, and temperature. As further density related data became available from the satellite accelerations due to drag, an improved atmospheric model, Jacchia 1971, was established. The J71 model includes density variations as a function of time and covers the altitude interval from 90-2500 km [Ref. 9]. It was adopted by the COSPAR working group as international reference

for the atmosphere in 1972 for heights ranging from 110 – 2000 km. The J71 model offers a reasonable description of the atmospheric density at moderate computational expense and is therefore widely used in orbit determination and prediction. [Ref. 9]

1.5.2 Jacchia-Roberts

The Jacchia-Roberts atmospheric model was originally derived from J70 and later modified according to J71. Robert's method is generally based upon the analytical solution of the barometric and diffusion differential equations which are obtained by the integration of partial differential equations. Robert's results match Jacchia exactly between 90 and 125 km and are in close agreement above 125 km. The advantage of Robert's modifications is that numerical integration is avoided and the computational speed is improved, [Ref. 10].

1.5.3 CIRA 1972

The COSPAR International Reference Atmosphere (CIRA) provides empirical models of atmospheric temperature and density from 0-2000 km. COSPAR periodically updates the atmospheric models. The first model was produced in 1965 (CIRA-65). The CIRA-72 atmospheric model included mean values from 25-500 km and Jacchia-71 prepared models from 110-2000 km. Data for this model originates from measurements of satellite drag and ground based observations [Ref. 11].

1.5.4 MSIS (Mass Spectrometer Incoherent Scatter models)

The Naval Research Laboratory has developed several empirical neutral atmospheric models based on data from satellites and high altitude rockets valid to an altitude of 1000 km. Mass spectrometers were integrated into the satellite hardware that produced in-situ measurements of chemical composition and temperature at upper atmospheric altitudes. Incoherent scatter radar techniques from ground based antennas provided measurements of atmospheric ion and electron properties that could be related to neutral atmosphere density and composition. The latest MSIS models are MSIS-86, MSISE-90, and NRLMSISE-00.

1.5.5 MSIS-86

The MSIS-86 model gives atmospheric properties based on data from rocket flights, satellites, and incoherent scatter radar data. Inputs to the model are year, day of year, universal time, altitude, geodetic latitude and longitude, local apparent solar time, solar $F_{10.7}$ flux (for previous day and three month average) and magnetic index A_p (daily or A_p history for last 59 hrs). The model outputs are neutral temperature at altitude, exospheric temperature, and densities of He, N_2, O_2, Ar, and H [Ref. 12].

1.5.6 MSISE-90

MSISE-90 has improvements over MSIS-86 incorporating additional data from sounding rockets, space flights, incoherent scatter results, and data used in the Jacchia models and not previously used in MSIS-86 [Ref. 12].

1.5.7 NRLMSISE-00

NRLMSISE-00 represents improvements over the earlier MSISE-90 model by including additional drag and accelerometer data from spacecraft, taking account of atomic oxygen, revising models of molecular and atomic oxygen in the lower atmosphere, and adding additional nonlinear terms to account for solar activity [Ref. 13].

1.6 Corrections to Atmospheric Density Models

The empirical atmospheric density models used to predict and determine the orbits of low Earth satellites exhibit large errors in density. These errors in density lead to errors in predicting the satellite motion in an orbit, which can affect other operations like estimating reentry, satellite maneuver planning, and collision avoidance. The errors in density from atmospheric models are due to solar and geomagnetic activity in the atmosphere. Generally, the solar flux data, $F_{10.7}$ (as a daily value), and geomagnetic activity index, K_p (as three hourly values), are used as inputs to all the models. The daily $F_{10.7}$ and three hourly K_p indices do not account for the continuous variations in the atmosphere, thus resulting in errors in density [Ref. 3]. Certain correction techniques to atmospheric density models were developed considering the continuous variations of solar and geomagnetic activity with time and other parameters of the atmosphere to generate improvements in density modeling for the empirical atmospheric models. Some of the methods for correcting atmospheric density models are discussed below. [Ref. 3]

1.6.1 Dynamic Calibration of the Atmosphere

Dynamic calibration of the atmosphere (DCA), started by Gorochov and Nazarenko in the 1980s, paved the way for a new approach in modeling atmospheric density [Ref. 14]. DCA makes corrections to a given density model using the observed motion of satellites. These observations come from a large number of satellites and are used to estimate corrections to a given density model. DCA uses the observation data from a set of calibration satellites in an orbit estimation process to generate orbital elements and satellite drag data. With the help of these data, a density model is constructed for the atmospheric variations inputting true ballistic coefficient. Later, corrections are generated to the atmospheric density from the constructed atmospheric model. In the High Accuracy Satellite Drag Model (HASDM) approach, corrections are generated every three hours, [Ref. 16]. These density corrections were then predicted forward in time three days by a time series filter as a function of predicted solar flux and geomagnetic indices. Using the predicted density, the predicted orbits were projected forward in time for three days. HASDM, which used the DCA approach to model atmospheric errors found improvements in predicting satellite positions and orbits, ballistic coefficient consistency and reduction of atmospheric density model errors when compared with existing atmospheric models [Ref. 16].

In addition to the improvements achieved by the DCA approach, it also has some drawbacks as described in references 17 and 18. The approaches are designed to run in real-time and internal to particular space surveillance architecture,

making outside users depend on that system to generate corrections. Also the DCA approach did not improve on the spatial and temporal resolution of existing models. Using daily solar flux values and three hour geomagnetic indices limits the ability of the models to represent changes in the atmosphere that occur within the averaging interval of input data, which affects the temporal resolution.

1.6.2 Accelerometers

A few satellites carry accelerometers onboard to measure non-conservative accelerations. The accelerometer measures the non-conservative forces such as Earth radiation pressure and solar radiation pressure. Modeling all the radiation pressure forces leaves only the atmospheric drag force, which can be used to estimate atmospheric density. The atmospheric density data from the accelerometers obtained are very accurate with precise temporal resolution. But, it has a poor spatial coverage because very few satellites carry accelerometers onboard [Ref. 19].

Two of the satellites analyzed in this research, the Challenging Minisatellite Payload (CHAMP) and the Gravity Recovery and Climate Experiment (GRACE) have accelerometers onboard providing much valuable data used in estimating atmospheric densities. In references 20 and 21, the accelerometer derived densities from these satellites were compared against the POE density estimates for various atmospheric models to check the consistency of the values.

The atmospheric density derived from the accelerometers proved to be more accurate than those obtained from an atmospheric model, provided accurate

force models are used to model the radiation forces [Ref. 20, 21]. Also, the accuracy of the densities mainly depends upon the performance and calibration of the instrument. The instrument must be corrected for maneuvers and instrumental bias, which can reduce the accuracy of data [Ref. 19].

1.6.3 Satellite Ephemerides

The work done in this research used satellite precision orbit ephemerides (POE) to make corrections to the atmospheric density models and generate estimated densities. Satellite precision orbit ephemerides (POE) are the data obtained from the Global Positioning System (GPS) receivers or from satellite laser ranging (SLR) observations. POE data can be obtained from GPS through the technique known as GPS accelerometry. References 22 through 24 describe the process of this approach for CHAMP and GRACE. The POE data consists of the precise position and velocity of a satellite for a given point of time. The obtained POE data are used in an orbit determination process to generate corrections to the atmospheric models and estimate the density. Work done by McLaughlin, Hiatt, and Lechtenberg in references 20, 21, 25, and 26 utilized the satellite POE data in generating corrections to atmospheric models. Reference 26 used the CHAMP POE data in order to derive atmospheric density estimates for periods of high solar activity. The orbit determination process in this research is performed with the Orbit Determination Tool Kit software (ODTK) developed by Analytical Graphics, Inc (AGI). The POE data are given as inputs in the ODTK software and are processed

through a sequential filter/smoother approach that outputs the estimated state and density of a given satellite. More explanation about this process is given in chapter 2.

1.7 Satellites Considered

Four different satellites ICESAT, TerraSAR-X, GRACE, and CHAMP were considered in this research. The ephemerides data of these satellites for various dates, various atmospheric models, and varying levels of solar and geomagnetic activity were used to generate corrected atmospheric densities. The details of these satellites are provided in the following subsections.

1.7.1 ICESat

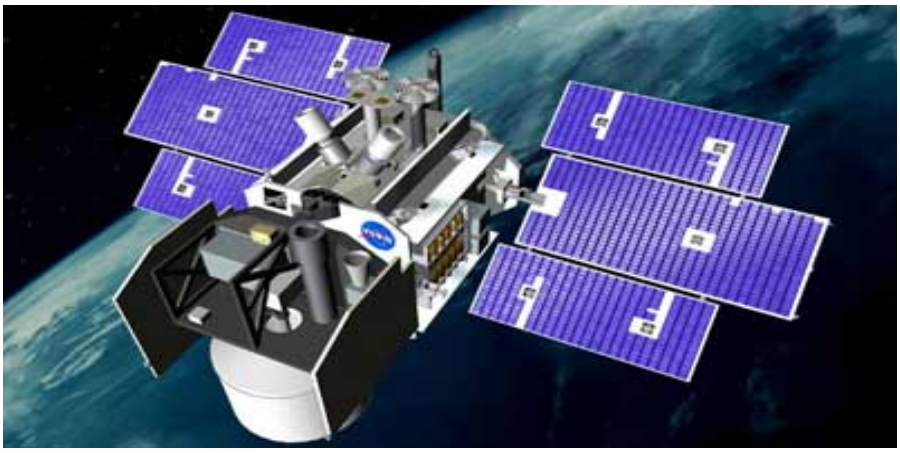

Fig 1.1 Image of ICESat in Orbit [Ref. 27]

ICESat (Ice, Cloud and Land Elevation Satellite) was launched on 13 January 2003 and decommissioned on 14 August 2010. ICESat reentered the atmosphere on 30 August 2010 [Ref. 27]. It orbited at an altitude of 600km and 94^{o} inclination. The

goal of the ICESat mission was to measure the changes in the polar ice sheet mass balance, provide elevation data of ice sheets, measure the distribution of clouds and provide cloud property information, and to map land topography and vegetation data around the globe. The primary instrument on ICESat is GLAS (Geoscience Laser Altimeter System) containing three lasers operating at certain intervals of time providing altimetry data of ice sheets and clouds, a GPS receiver, and a star tracker attitude determination system [Ref. 27]. The POE data of ICESat from the years 2003 to 2008 were used in this research for estimating atmospheric density values.

1.7.2 TerraSAR-X

Fig 1.2 Image of TerraSAR-X in orbit [Ref. 28]

TerraSAR-X (Terra Synthetic Aperture Radar- X band), a German Earth observation satellite was launched on 15 June 2007. It orbits at an altitude of 514 km in a polar orbit with 97.44^{o} inclination [Ref. 28]. TerraSAR-X was launched with a mission to

acquire high-quality radar images of the Earth with the help of its active phased array X-Band SAR antenna on board. TerraSAR-X is designed to carry out its task for five years. In this research the POE data of TerraSAR- X for certain days from 2007-2010 were used in estimating atmospheric densities [Ref. 28].

1.7.3 CHAMP

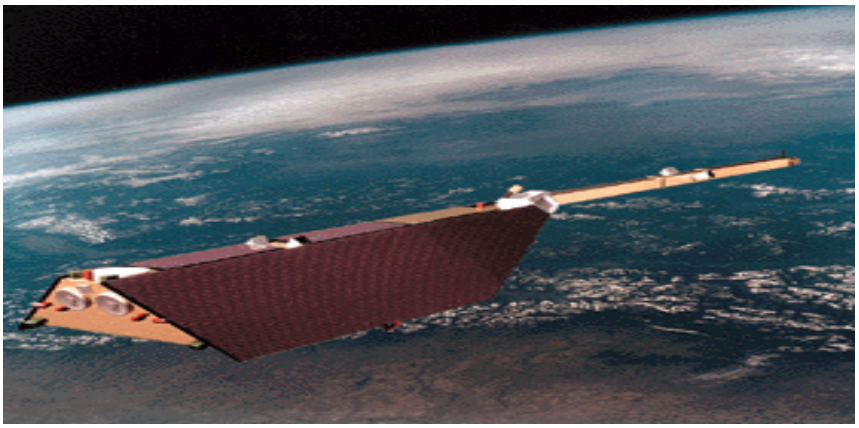

Fig 1.3 Image of CHAMP satellite in orbit [Ref. 29]

The Challenging Mini-Satellite Payload (CHAMP) was launched on 15 July 2000 and scheduled to last for five years [Ref. 29]. It was used for geophysical research and application by providing a sufficiently long observation time to resolve long-term temporal variations primarily in the magnetic field, in the gravity field, and within the atmosphere. The satellite re-entered the Earth's atmosphere on 20 September 2010. It carries the Spatial Tri-axial Accelerometer (STAR) for research. The POE data from

CHAMP for the years 2003-2009 was used in this research to estimate atmospheric density [Ref. 29].

1.7.4 GRACE

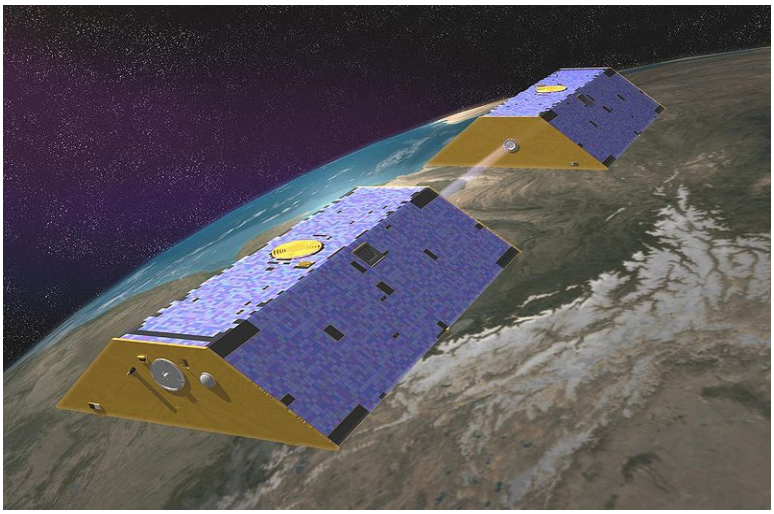

Fig 1.4 Image of GRACE satellites in orbit [Ref. 30]

The Gravity Recovery and Climate Experiment (GRACE) satellites were launched on 17 March 2002 with an objective to study the gravity variations of Earth and create a better profile of the Earth's atmosphere [Ref. 30]. The GRACE mission has two identical spacecraft flying 220 km apart at an altitude of 500 km above Earth and is able to map the Earth's gravity fields by making accurate measurements of the distance between the two satellites using GPS and a microwave ranging system. These satellites have accelerometers on board, the data from which was used in this research to compare with POE atmospheric densities [Ref. 30].

2 Methodology

This chapter explains the methods used in this research to obtain the atmospheric density estimates from precision orbit ephemerides (POE) with the help of the Orbit Determination Tool Kit (ODTK) software. The densities were estimated using various baseline atmospheric density models, different density and ballistic coefficient correlated half-life combinations, and for days with varying levels of solar and geomagnetic activity. The estimated densities were compared with the densities derived from accelerometers onboard CHAMP and GRACE to check their accuracy. A brief introduction to orbit determination and precision orbit ephemerides is given to provide a better understanding of the methods used in this research.

2.1 Precision Orbit Ephemerides (POE)

The ephemerides of a satellite are a set of values that give the position and velocity vectors of a satellite at given points in time. The units of these values used in this work are meters (m) for position values and meters/sec (m/s) for velocity values. Generally, the ephemerides are calculated from the mathematical equations which describe the motion of a satellite, based on observations. Nowadays with the advance of technology, the Global Positioning System (GPS) is used in obtaining accurate ephemeris data for satellites. Satellites equipped with GPS onboard circle around the earth in very precise orbits and transmit signals containing the ephemeris data to Earth. The signal transmitted by the satellite contains information about the ephemeris data like position, velocity, current date, and time.

The POE data for the CHAMP, GRACE, ICESat, and TerraSAR-X satellites are used in this research. The ICESat POE data were obtained from the Center for Space Research at the University of Texas, Austin which carries out the calibration and validation for the ICESat data. The POE data for CHAMP, GRACE, and TerraSAR-X were obtained from Information System and Data Centre (ISDC) which carries out its research on Earth sciences from the data obtained from these satellites and is a part of German National Research Centre for Geo Sciences (GFZ) at Potsdam, Germany.

2.2 Orbit Determination

The information presented in this section is summarized from references 31 through 34. “Orbit determination refers to the process of estimating or predicting the orbit of a spacecraft or a celestial body orbiting around a central body”, Ref. [31]. In this work, it refers to the motion of a satellite around the Earth. Orbit determination is very important for many satellite missions. Having knowledge about satellite position at a given time is required for various satellite applications like weather monitoring, navigation, communication, and mission planning. In order to receive better measurements from satellite applications, an accurate estimate of the satellite orbit is required. Satellites in orbit are affected by many non-gravitational and gravitational forces which result in errors in predictions. An accurate atmospheric model is needed to model these forces and increase the accuracy in orbit predictions.

To predict the orbit of a satellite, some observations from the motion of the satellite with time are required which are related to the satellite's position and velocity. The position and velocity vectors along with force models and measurement parameters form the basic set of parameters in the initial state vector required to predict the motion of a satellite for satellite orbit determination. Other than the set containing position and velocity vectors, another elemental set containing Keplerian elements can also be used to predict the satellite orbit.

The state of a satellite at some point in the future can be calculated by using the differential equations that govern the motion of the satellite provided the initial state of the satellite at some initial time is known. The equations of motion along with a numerical integration technique can be used to integrate the equations of motion and obtain the state of the satellite at any time in the future. Since the initial state vector of a satellite and the force models and measurement parameters are just approximations and are not exactly known, this result in an error in the prediction of the satellite motion. These errors in prediction grow over of time. Therefore, observations of the satellite such as range, range-rate, azimuth, and elevation from tracking stations whose positions are accurately known are used to continually update the satellite's state vector thus resulting in an increase in the accuracy of satellite prediction.

In this research the POE data from satellites are used as measurements to determine the orbit of a satellite. Position vectors in POE serve as inputs for a

sequential Kalman filter/smoother approach using Gauss-Markov processes, which are discussed in the subsequent section.

2.3 Gauss-Markov Process Half-Lives

Generally the term half life is defined as the time required for a value or product to decay to half of its initial value. The half-life determines how long past corrections affect the current corrections. There are at least two sources of air-drag acceleration error while estimating density. They are the errors in atmospheric density and in the ballistic coefficient, Ref [35, 36]. Both errors must be estimated and corrected for a better orbit determination process. In Orbit Determination Tool Kit (ODTK) software there are two parameters called density correlated half-life and ballistic coefficient correlated half-life which can be adjusted by the user as a part of the force models. The density and ballistic coefficient half-lives given in ODTK determine the amount of time required for the propagating error between measurements to decay to half of its value, Ref [35, 36].

Reference 37 provides information about half-lives in ODTK as follows. In ODTK density is denoted by ρ and the estimated correction to density is denoted by $\Delta\rho/\rho$. Similarly, ballistic coefficient is denoted by B and the estimated correction to ballistic coefficient is $\Delta B/B$. The density correlated half-life is the time required for the estimated correction to the atmospheric drag ($\Delta\rho/\rho$) to decay to half of its value in the absence of measurement data represented in units of time. In the same way the ballistic coefficient correlated half-life is the time required for the estimated correction to the ballistic coefficient to decay to half its value in absence of

measurement data represented in units of time. The density and ballistic coefficient correlated half-life values are associated with the exponential half-life in the Gauss-Markov processes used by ODTK, Ref [37, 38].

In reference 31, the Gauss-Markov sequence is explained as follows. Let $x = x(t_k)$ denote a dynamic scalar random variable (density or ballistic coefficient) that satisfies the Gauss-Markov equation

$$x(t_{k+1}) = \phi(t_{k+1}, t_k)x(t_k) + \sqrt{1-\phi^2(t_{k+1}, t_k)}w(t_k), k \in \{0,1,2,...\} \quad (2.1)$$

w(t) is a Gaussian white noise variable with zero mean and constant variance. The initial value for *w(t)* is equal to the initial value of a scalar random variable.

$$x(t_0) = w(t_0) \quad (2.2)$$

The transformation function is defined as

$$\phi(t_{k+1}, t_k) = e^{\alpha t_{k+1}, t_k} \quad (2.3)$$

The constant in the transition function is given by

$$\alpha = (\ln 0.5)/\tau \quad (2.4)$$

The constant depends on the user defined half-life value, τ, in ODTK.

The half life values used for density and ballistic coefficient in this research are 1.8, 18, 180 minutes. These values for the half-lives were varied by an order of ten to examine how the increase in half-life values affects the orbit determination.

2.4 Filter-Smoother

"The Kalman filter is a set of mathematical equations that provides an efficient computational means to estimate the state of a process in a way that minimizes the error", Ref [39]. The filter is powerful for supporting estimates of past, present, and future states even when the precise nature of the modeled system is unknown. More information on the Kalman filter can be found from reference [39].

In ODTK, an optimal sequential filter is used, which runs the input POE data and estimates orbits with measurement updates similar to a Kalman filter, enabling the calculation and propagation of realistic error covariance. The sequential filter is initialized with an initial epoch, initial state estimate, measurement data to update the state estimate, and all supporting data and model parameters to operate the filter process, Ref [40]. The filter processes the measurements sequentially forward in time resulting in outputs that consist of a complete state estimate and error covariance, which are again used as the initial conditions for their forward propagation.

The filter includes a smoother, which provides a smoothed ephemeris. The input measurement for the smoother is the filtered output. A fixed interval smoother post-processes the filter output to create a more accurate and continuous definitive satellite ephemeris that results in an estimate of the orbit solution and biases with a realistic understanding of their accuracy. Smoothed estimates are more accurate when compared to filter estimates, since it makes use

of both future and past data. Ref [40] provides more information on the ODTK filter-smoother process.

2.5 Cubic Spline Interpolation

Interpolation is a method to estimate a set of values between two given values. The process involves the construction of a smooth curve that fits best for those values. There are different types of interpolation techniques such as linear interpolation, polynomial interpolation, and spline interpolation. Of these methods, spline interpolation, especially cubic spline interpolation, is the most popularly used method. “The cubic spline interpolation is a piecewise continuous curve, passing through each of the values in the table. A cubic spline has minimum oscillatory behavior which results in smooth transitions between data points”, Ref. [42].

The behavior of the atmosphere is primarily influenced by space weather data. Measurements or predicted values of these data are given as inputs to an atmospheric density model to calculate the atmospheric density at the location of the satellite. The atmospheric data thus obtained are used to calculate the atmospheric drag force on the satellite. Small changes in space weather data can have a large effect on the propagation of a satellite in orbit. The space weather data consists of the solar and geomagnetic indices. These indices provide atmospheric models with the necessary information to predict the atmospheric density for orbital calculations. There has been significant study over the years about the impact of imperfect modeling by the existing atmospheric models on the atmospheric density values.

There is a need to input more short term space weather data values into the model than the currently used three hourly or daily values, Ref [41,42, 43, and 44].

In reference [42] several interpolation approaches for space weather data were explored including linear interpolation, an iterative approach, and a splining approach. “The closure of iterative, interpolated, and cubic splining values was exact, but the spline technique showed some small variations. The cubic spline technique was found to best replicate the observed data values, while simultaneously maintaining closure properties” [Ref. 42].

In this research the cubic spline interpolation is performed within ODTK on the geomagnetic index data values which are normally available as three hourly or daily values. Using cubic spline interpolation for the geomagnetic index values, the atmospheric density models can be modeled effectively resulting in more accurate estimated densities.

2.6 Deriving Atmospheric Density Estimates Using ODTK

In this research, the atmospheric densities are estimated by correcting the existing atmospheric density models in ODTK. The following subsections describe how the ODTK is used to estimate the corrections to density and ballistic coefficient values for various cases.

2.6.1 ODTK Software

ODTK is the orbit determination software used in this research to estimate POE densities by generating corrections to atmospheric models. The ODTK software provides orbit determination and orbit analysis support by estimating satellite state and environment parameters. In ODTK, the sequential filter with filter/smoother approach can refine the data and produce accurate values, Ref [36]. In ODTK a variation of parameters numerical integrator is used with full force models to propagate the orbit, Ref [37]. The force models include a GRACE Gravity Model GGM02C, solid Earth and ocean tides, Jacchia and MSIS family atmospheric drag models, effects from solar radiation pressure and third body effects of the Sun and Moon. ODTK also calculates corrections to atmospheric density and ballistic coefficient.

2.6.2 Estimating Atmospheric Density using ODTK

In the ODTK software, a scenario is created for the desired date and time interval. The scenario consists of all the data regarding the force models, measurement models, state inputs, solar flux, geomagnetic index, gravity models, orbit state, Earth reference frame, physical properties of the satellite, satellite attitude, ranging method, perturbations, satellite characteristics, GPS clock, filter and smoother. After creating the ODTK scenario, the POE data obtained from the desired satellite is input. Before inputting the POE data it is converted into a Navigation Solution (NAVSOL) file format, the format which ODTK can read. After inputting

the POE data file, the scenario is run with the help of a user generated script in the ODTK scripting tool. The script can be modeled according to the user requirements for particular models and half-lives. ODTK runs the scenario and processes the data using the filter/smoother approach, models all the forces and perturbations, performs integration and outputs the estimated density values for various atmospheric density models and also for different ballistic coefficient and density correlated half-lives.

The estimated density values for different models are checked for their accuracy by comparing them with the values derived from accelerometers when available. Also the estimated density values for all the satellites and different atmospheric models used in this research were plotted to observe which model performs best for a given set of conditions. The density estimates obtained can be used to obtain accurate drag estimates on a satellite and also for better orbit determination.

2.7 Estimation of Atmospheric Density for Different Cases

The estimated atmospheric densities are obtained as a result of corrections made to the existing atmospheric models in ODTK. In this research the corrected atmospheric densities are estimated for three different factors by varying the baseline atmospheric density model, varying the density and ballistic coefficient correlated half-lives, and estimating density for varying levels of solar and geomagnetic activity. The results from each of these cases were compared to the results from accelerometer and empirical density models corresponding to the same case.

2.7.1 Varying the Baseline Atmospheric Density Model

There are five atmospheric density models available in the ODTK software. They are CIRA-72, Jacchia-71, Jacchia-Roberts, MSISE-90, and NRLMSISE-00. In this research corrections are made to two models (CIRA-72 and NRLMSISE-00) picking one from the Jacchia family of models and the other from the MSIS family. The POE density estimates are obtained by generating corrections to these atmospheric models. The POE densities obtained using both the models are examined to see how the density estimates obtained using POE data vary for each model. Also, the POE densities are compared to the empirical Jacchia model densities to observe the difference between them. For the satellites, that have accelerometers on-board, the POE densities are compared with the accelerometer densities to check the correlation.

2.7.2 Varying the Density and Ballistic Coefficient Correlated Half-Lives

The densities were estimated for different combinations of density and ballistic coefficient correlated half-lives. Both the density and ballistic coefficient correlated half-lives were varied by orders of magnitude with values of 1.8 minutes, 18 minutes, and 180 minutes. In this research the density estimates were found for two different cases of half-life combinations. One combination is by keeping the density correlated half-life constant and varying the ballistic coefficient correlated half-life and the other is vice-versa. The POE densities obtained by varying different half-life combinations are observed to see how the variations in half-lives affect the

POE densities. All these combinations were examined for each of the two atmospheric density models mentioned in the above section to determine which half-life combination and atmospheric model together yields a better estimation of density and also to determine the consistency in density changes among satellites as parameters are changed.

2.7.3 Varying Levels of Solar and Geomagnetic Activity

The POE densities were estimated for different days during which the satellites GRACE, CHAMP, ICESAT, and TerraSAR-X were active in orbit. Days were selected covering all the levels of magnitude for solar and geomagnetic activity classifying them into seven different bins as shown in Table 2.1. They are low, moderate, and active for geomagnetic activity; and low, moderate, elevated, and high for solar activity.

Solar Activity	**Solar Flux ($F_{10.7}$)**	**Geomagnetic Activity**	**Daily Planetary Amplitude (A_p)**
Low	$F_{10.7}$ <75	Quiet	A_p<10
Moderate	75< $F_{10.7}$ <150	Moderate	10<A_p<50
Elevated	150< $F_{10.7}$ <190	Active	50<A_p
High	190< $F_{10.7}$		

Table 2.1 Solar and Geomagnetic activity Bins, Ref [7, 8]

Densities were estimated for all the seven bins for different satellites and the effect of these varying magnitudes on atmospheric density were studied. This gives a better understanding of how the densities vary for a period of low, moderate and high

activities. This is very important to study how the densities in the atmosphere change especially during increased solar activity and how the actual densities vary from the values estimated by the existing atmospheric models.

2.8 Validation of Estimated Atmospheric Density

In order to check the accuracy of the POE estimated density values obtained through ODTK, they are compared with the density values derived from accelerometers on-board the satellites. The accelerometer derived density values are considered to be the accurate values since they are directly derived from the data obtained from accelerometers. In this research, the correlation between the POE density estimates and the accelerometer densities are found by finding the cross correlation (CC) and root mean square (RMS) values between them. CC and RMS values give the degree of correlation between the estimated density values and the accelerometer density values. For satellites which do not possess accelerometers on board like ICESAT and TerraSAR-X, the POE density estimates are plotted along with the empirical model densities to observe the variation.

2.8.1 Cross Correlation (CC)

Cross correlation is a method used to determine the degree of correlation between two different time varying quantities. In this research, cross correlation coefficient was calculated for the POE density estimates compared with the accelerometer density and also for the Sutton accelerometer density compared

with Bruinsma accelerometer density. The range of cross correlation values is from -1 to 1. A cross correlation coefficient value near 1 indicates a higher degree of correlation between the data sets. If it is close to -1 the data sets are negatively correlated and a value of zero indicates no correlation.

Reference [46] gives the equation for cross correlation as follows. For example, consider two sets of data $x(i)$ and $y(i)$ where $i = 0,1,2,....,N-1$ and N represents the number of elements in each set, then the cross correlation, *r*, between the two sets is given as

$$r(d) = \frac{\sum_{i=0}^{N-1}[(x(i)-mx)*(y(i-d)-my)]}{\sqrt{\sum_{i=0}^{N-1}(x(i)-mx)^2}\sqrt{\sum_{i=0}^{N-1}(y(i-d)-my)^2}} \qquad (2.5)$$

Where mx and my in the above equation are mean values for each set and d is the delay, defined as d=0, 1,…..N-1.

2.8.2 Root Mean Square (RMS)

Like CC, RMS is another method of comparing two sets of estimated density values. Generally, RMS is defined as the square root of the arithmetic mean of the squares of a set of values. If x_i is a data set for i=0,1….n, then RMS is given as

$$RMS = \sqrt{\frac{x_1^2 + x_2^2 + x_3^2 + ...x_n^2}{n}} \qquad (2.6)$$

RMS is a good method to find out the precision between two data sets. RMS values show by how much one set of data deviates from another set. The closer the value of RMS to zero the better is the precision of the values. In this research we used RMS error or RMS deviation to find out the magnitude of difference that exists between two sets of data. If x_i and y_i are two sets of data for i=0,1,2…..n, then the Root Mean Square Error (RMSE) is given as

$$RMSE(x,y) = \sqrt{\frac{\sum_{i=1}^{n}(x_i - y_i)^2}{n}} \qquad (2.7)$$

The RMS values calculated for density in this research will possess units of 10^{-12} kg/m^3.

2.9 Conclusion

The main objective of this research is to generate corrections to the atmospheric density models by using satellite POE. The methods used to obtain and validate POE density estimates by generating corrections to the atmospheric models are discussed in this chapter. Chapter 4 in this work will use the methodology in this chapter to generate corrections to the atmospheric models. Chapter 4 presents the work done on generating POE density estimates from POE data provided by the ICESAT and TerraSAR-X satellites which is an extension of the work done in Ref [20, 21]. Chapter 3 mainly focuses on comparing two sets of accelerometer derived densities from the CHAMP and GRACE accelerometers.

3 Comparison of Sutton and Bruinsma Accelerometer Derived Densities for the CHAMP and GRACE Satellites

This chapter examines the accelerometer densities of CHAMP and GRACE derived by Eric Sutton, from the University of Colorado. The densities derived by Sutton are compared with the accelerometer densities derived by Sean Bruinsma from CNES, Department of Terrestrial and Planetary Geodesy, France. The cross correlation and root mean square (RMS) values of both densities were found to determine the proximity between Sutton derived densities and Bruinsma derived densities. The Bruinsma derived densities are considered as reference values in this work.

Both, Bruinsma and Sutton derived the atmospheric densities for CHAMP and GRACE using the measurements from accelerometers on board the satellites. References [20] and [21] used the densities derived by Bruinsma to validate the POE density estimates obtained in their work. The work presented in this chapter determines the closeness of Sutton's densities to those of Bruinsma. If Sutton's densities are found to be well correlated with the Bruinsma densities, then they can be used as a substitute for Bruinsma's densities in future validations of POE density estimates. This also gives confidence in the use of densities from either source.

Sutton's densities were compared to Bruinsma's densities for different operational days of the CHAMP and GRACE satellite missions. The days selected for comparison cover a wide range of solar and geomagnetic activity. The selected days were classified into seven different bins depending on the type of solar

and geomagnetic activity as mentioned in section 1.3.4 of Chapter 1 and the corresponding CC and RMS average values were found. The CC and RMS values obtained show the correlation of Sutton and Bruinsma derived densities and also help to observe the variation of correlation for different types of solar and geomagnetic activity. A brief explanation about deriving the densities from the accelerometers of the CHAMP and GRACE satellites is presented in the following section.

3.1 Derivation of Densities from Accelerometers Onboard the CHAMP and GRACE Satellites

Both the CHAMP and GRACE satellites carry a STAR accelerometer on board. The STAR accelerometer measures the sum of all non-conservative forces acting on the satellite. The forces measured by the accelerometer are comprised of many forces like atmospheric drag, solar radiation pressure (SRP), Earth albedo radiation pressure, and infrared radiation (IR) pressure. Atmospheric drag is the main force of concern here. The atmospheric density is obtained from the accelerometer measurements by calculating the drag component acting on the satellite, since atmospheric density is proportional to the drag force. In order to find the drag force from the accelerometer measurements, the forces other than atmospheric drag have to be eliminated from the obtained measurements. Therefore, the effects of SRP, Earth albedo, and Earth IR are removed by modeling the forces to get drag accelerations and then the atmospheric density can be calculated from the drag accelerations by modeling the drag coefficient.

References 19, 47 and 48 explain the methods employed by Bruinsma and Sutton to retrieve measurements from the accelerometers and derive the density values from those obtained accelerometer measurements. They also provide the results of validation for derived accelerometer densities by comparing them with the densities obtained from atmospheric models. The error between the compared densities ranged from 15% - 30% depending on the type of solar and geomagnetic activity.

3.2 Sutton and Bruinsma Accelerometer Derived Density Comparison

The CC and RMS values between the Sutton and Bruinsma densities for different days covering a wide range of solar and geomagnetic activity levels were found for both CHAMP and GRACE. The CC values show the correlation and the RMS values show the precision between two density data sets. Later, the selected days were classified into seven different bins depending on the solar and geomagnetic activity levels and CC and RMS values were averaged for those bins. The days selected in this work were randomly picked from a pool of available dates for the CHAMP and GRACE missions covering various levels of solar and geomagnetic activity and also to cover some of the days used in reference 21, which could be helpful for future work. The CC values have no units and all the RMS values have units of 10^{-12} kg/m^3. The time series for Bruinsma and Sutton density sets are different; therefore the Sutton density values were interpolated to match the time series for the Bruinsma density sets.

3.2.1 CC and RMS Values between Sutton and Bruinsma Accelerometer Derived Densities for Selected Days of the CHAMP Mission

Days were selected from the years 2001-2007 consisting of all levels of solar and geomagnetic activity for CHAMP and CC and RMS values were found for those days. Tables 3.1 to 3.7 show the selected days and their corresponding CC and RMS values along with Solar Flux and Geomagnetic indices.

Table 3.1: Selected Dates for CHAMP and corresponding CC and RMS values for the year 2001. ***All RMS values are given in 10^{-12} kg/m^3***

Year	Month	Day	A_p	$F_{10.7}$	CC	RMS
2001	Jun	17	7	204.6	0.995	0.765
2001	Jun	18	36	221.3	0.990	0.765
2001	Jun	19	12	195.4	0.995	0.767
2001	Jul	20	4	142.6	0.976	0.822
2001	Jul	27	6	121.4	0.982	0.825
2001	Jul	30	7	114.5	0.975	0.763
2001	Oct	1	48	216.5	0.981	0.714
2001	Oct	2	52	200.9	0.979	0.694
2001	Oct	3	69	191.7	0.983	0.659
2001	Oct	22	96	232.7	0.975	0.641
2001	Nov	5	21	234.6	0.991	0.658
2001	Nov	6	142	237.4	0.972	0.717

Table 3.2: Selected Dates for CHAMP and corresponding CC and RMS values for the year 2002. ***All RMS values are given in 10^{-12} kg/m^3***

Year	Month	Day	A_p	$F_{10.7}$	CC	RMS
2002	Apr	15	6	203.6	0.984	0.249
2002	Apr	17	62	193.8	0.963	0.495
2002	Apr	19	62	179.2	0.933	0.528
2002	Apr	20	70	177.5	0.962	0.389
2002	Apr	23	27	175.3	0.982	0.276
2002	Sep	6	7	178.1	0.992	0.288
2002	Sep	7	57	182.8	0.991	0.592
2002	Sep	30	28	139.7	0.992	0.304
2002	Oct	1	67	139.8	0.964	0.491
2002	Oct	2	53	135.8	0.989	0.380
2002	Oct	3	45	145.9	0.989	0.347
2002	Oct	23	11	163.6	0.990	0.243

Table 3.3: Selected Dates for CHAMP and corresponding CC and RMS values for the year 2003. ***All RMS values are given in 10^{-12} kg/m^3***

Year	Month	Day	A_p	$F_{10.7}$	CC	RMS
2003	Jan	7	6	163.2	0.987	0.197
2003	Jan	8	4	172.7	0.989	0.110
2003	Feb	1	14	125.8	0.983	0.219
2003	Feb	2	52	126.2	0.969	0.326
2003	Mar	19	12	108.2	0.973	0.108
2003	Mar	20	25	97.4	0.950	0.212
2003	May	28	34	130.2	0.983	0.241
2003	May	29	109	137.8	0.986	0.289
2003	Jun	17	49	121.9	0.984	0.211
2003	Jun	18	60	120.4	0.985	0.223
2003	Jul	10	7	122.8	0.993	0.113
2003	Jul	11	52	122	0.972	0.249
2003	Aug	17	20	119.3	0.965	0.194
2003	Aug	20	17	111.8	0.986	0.086
2003	Aug	21	58	119.2	0.966	0.236
2003	Sep	16	34	99.3	0.982	0.321
2003	Oct	30	191	271.4	0.956	0.930
2003	Oct	31	116	280.9	0.983	0.694
2003	Nov	1	26	210.4	0.988	0.289
2003	Nov	20	150	170.2	0.984	0.839

Table 3.4: Selected Dates for CHAMP and corresponding CC and RMS values for the year 2004. ***All RMS values are given in 10^{-12} kg/m^3***

Year	Month	Day	A_p	$F_{10.7}$	CC	RMS
2004	Jan	15	18	119.1	0.974	0.182
2004	Jan	16	29	120.3	0.980	0.168
2004	Jul	20	8	175.2	0.990	0.178
2004	Jul	21	4	172.2	0.991	0.152
2004	Jul	26	47	128	0.981	0.282
2004	Oct	31	42	89.9	0.987	0.221
2004	Nov	2	4	133.1	0.993	0.190
2004	Nov	3	10	135.9	0.991	0.186
2004	Nov	8	140	124.1	0.974	0.900
2004	Nov	9	119	140.9	0.979	0.342

Table 3.5: Selected Dates for CHAMP and corresponding CC and RMS values for the year 2005. ***All RMS values are given in 10^{-12} kg/m^3***

Year	Month	Day	A_p	$F_{10.7}$	CC	RMS
2005	Jan	16	16	144.5	0.951	0.138
2005	Jan	17	58	137.5	0.944	0.483
2005	Jan	19	60	132.5	0.958	0.328
2005	Jan	21	56	113.5	0.959	0.512
2005	Mar	11	5	104.9	0.991	0.234
2005	Mar	16	6	104.6	0.991	0.243
2005	Mar	18	10	96.5	0.988	0.276
2005	Apr	4	26	84.8	0.982	0.269
2005	May	10	7	119.2	0.983	0.196
2005	May	11	12	125.7	0.932	0.375
2005	May	30	90	94.9	0.947	0.552
2005	Jun	12	54	103	0.971	0.381
2005	Jun	22	6	79.5	0.981	0.211
2005	Jul	9	24	109.6	0.983	0.293
2005	Jul	10	57	101.8	0.972	0.512
2005	Aug	23	7	106.9	0.992	0.126
2005	Aug	24	102	98.6	0.992	0.116
2005	Sep	10	33	116	0.984	0.200
2005	Sep	11	101	109.7	0.992	0.124
2005	Oct	25	21	73.1	0.981	0.117
2005	Oct	28	5	73	0.989	0.124

Table 3.6: Selected Dates for CHAMP and corresponding CC and RMS values for the year 2006. ***All RMS values are given in 10^{-12} kg/m^3***

Year	Month	Day	A_p	$F_{10.7}$	CC	RMS
2006	Aug	2	9	72.1	0.987	0.134
2006	Aug	3	5	71.3	0.991	0.103
2006	Aug	4	2	69.6	0.990	0.089
2006	Dec	21	2	83.8	0.980	0.182
2006	Dec	22	2	83.7	0.985	0.161
2006	Dec	23	16	72.7	0.985	0.154
2006	Dec	24	12	73.5	0.989	0.128

Table 3.7: Selected Dates for CHAMP and corresponding CC and RMS values for the year 2007. ***All RMS values are given in 10^{-12} kg/m^3***

Year	Month	Day	A_p	$F_{10.7}$	CC	RMS
2007	Sep	8	6	66.6	0.990	0.123
2007	Sep	9	2	66.7	0.992	0.106
2007	Sep	10	2	66.9	0.991	0.106
2007	Sep	11	3	66.1	0.990	0.165

In tables 3.1 to 3.7, the CC values are found to be around 0.95- 0.99 for all types of solar and geomagnetic activity for the CHAMP satellite. This indicates that the Sutton accelerometer densities correlated well with the Bruinsma accelerometer densities. Although the CC values exhibited a slight variation between low, moderate and high solar and geomagnetic activities, that variation is very small. The days with low and moderate solar and geomagnetic activity have CC value around 0.97-0.99 while the days with high and elevated solar and geomagnetic activity have the CC value around 0.95-.97.

The RMS values are around 0.05-0.2 x10^{-12} kg/m^3 for low and moderate solar and geomagnetic activity and are around 0.3-0.8 x10^{-12} kg/m^3 for

active geomagnetic and high solar activity. The RMS values are close to zero for periods of low and moderate solar and geomagnetic activity. But, for the periods of active geomagnetic activity, and high and elevated solar activity the RMS values worsened almost doubling when compared to the low and moderate cases. This is primarily because the densities are higher. The RMS values indicate a high degree of precision between the Sutton and Bruinsma densities for low and moderate periods of solar and geomagnetic activity and a lower degree of precision for high and elevated levels of activity.

3.2.2 CC and RMS Values between Sutton and Bruinsma Accelerometer Derived Densities for Selected Days of the GRACE Mission

Days were selected from the years 2003-2007 consisting of all levels of solar and geomagnetic activity for GRACE and CC and RMS values were found for those days. The tables from 3.8 to 3.12 show the selected days and their corresponding CC and RMS values along with solar flux and geomagnetic indices.

Table 3.8: Selected Dates for GRACE and corresponding CC and RMS values for the year 2003. ***All RMS values are given in 10^{-12} kg/m^3***

Year	Month	Day	A_p	$F_{10.7}$	CC	RMS
2003	May	28	34	130.2	0.984	0.239
2003	May	29	109	137.8	0.975	0.280
2003	Jun	17	49	121.9	0.975	0.222
2003	Jul	11	52	122	0.982	0.212
2003	Aug	20	17	111.8	0.982	0.106
2003	Aug	21	58	119.2	0.986	0.193
2003	Oct	30	191	271.4	0.966	0.685
2003	Oct	31	116	280.9	0.959	0.610
2003	Nov	1	26	210.4	0.962	0.402
2003	Nov	20	150	170.2	0.977	0.737

Table 3.9: Selected Dates for GRACE and corresponding CC and RMS values for the year 2004. ***All RMS values are given in 10^{-12} kg/m^3***

Year	Month	Day	A_p	$F_{10.7}$	CC	RMS
2004	Jul	20	8	175.2	0.972	0.306
2004	Jul	21	4	172.2	0.978	0.392
2004	Oct	31	42	89.9	0.984	0.216
2004	Nov	8	140	124.1	0.978	0.556
2004	Nov	9	119	140.9	0.963	0.318

Table 3.10: Selected Dates for GRACE and corresponding CC and RMS values for the year 2005. ***All RMS values are given in 10^{-12} kg/m^3***

Year	Month	Day	A_p	$F_{10.7}$	CC	RMS
2005	Jan	16	16	144.5	0.990	0.133
2005	Jan	17	58	137.5	0.968	0.254
2005	Jan	19	60	132.5	0.980	0.240
2005	Jan	21	56	113.5	0.981	0.224
2005	Mar	11	5	104.9	0.992	0.134
2005	Mar	18	10	96.5	0.986	0.156
2005	May	10	7	119.2	0.989	0.137
2005	May	11	12	125.7	0.980	0.123
2005	Jun	12	54	103	0.973	0.125
2005	Jul	9	24	109.6	0.982	0.114
2005	Jul	10	57	101.8	0.968	0.182
2005	Aug	23	7	106.9	0.987	0.141
2005	Aug	24	102	98.6	0.986	0.139
2005	Sep	10	33	116	0.965	0.169
2005	Sep	11	101	109.7	0.986	0.248
2005	Oct	25	21	73.1	0.989	0.180

Table 3.11: Selected Dates for GRACE and corresponding CC and RMS values for the year 2006. ***All RMS values are given in 10^{-12} kg/m^3***

Year	Month	Day	A_p	$F_{10.7}$	CC	RMS
2006	Aug	2	9	72.1	0.991	0.099
2006	Aug	3	5	71.3	0.994	0.081
2006	Aug	4	2	69.6	0.990	0.093
2006	Dec	22	2	83.7	0.983	0.090
2006	Dec	23	16	72.7	0.986	0.086

Table 3.12: Selected Dates for GRACE and corresponding CC and RMS values for the year 2007. ***All RMS values are given in 10^{-12} kg/m^3***

Year	Month	Day	A_p	$F_{10.7}$	CC	RMS
2007	Sep	8	6	66.6	0.995	0.083
2007	Sep	9	2	66.7	0.989	0.098
2007	Sep	10	2	66.9	0.989	0.086
2007	Sep	11	3	66.1	0.988	0.077

Tables 3.8 to 3.12 show the CC and RMS values for the selected days from the year 2003-2007 for GRACE. The CC and RMS values for the GRACE satellite are similar to those of CHAMP satellite. The CC values were found to be around 0.95–0.99 for all levels of solar and geomagnetic activity and the RMS values ranged between 0–0.2 for low and moderate solar activity and geomagnetic activity, and between 0.2–0.7 for active, elevated, and high solar and geomagnetic activity.

For the days with high solar and geomagnetic activity the correlation between the densities worsened slightly when compared with the densities for the days of low activity. This can be seen from the CC and RMS values obtained. Overall, these CC and RMS values indicate that the Sutton accelerometer densities correlated well with the Bruinsma accelerometer densities for GRACE.

3.2.3 Averaged CC and RMS Values Binned According to the Type of Solar and Geomagnetic Activity for the Selected Days

The CC and RMS values from the tables 3.1 to 3.12 are sorted out in bins according to the type of solar and geomagnetic and are averaged for both CHAMP and GRACE. Tables 3.13 and 3.14 show the average CC and RMS values for each bin separately for CHAMP and GRACE.

Table 3.13: Averaged CC and RMS values for the selected days of CHAMP and GRACE missions for different levels of geomagnetic activity. *All RMS values are given in 10^{-12} kg/m^3*

Geomagnetic activity	Index	CHAMP		GRACE	
		Avg CC	Avg RMS	Avg CC	Avg RMS
Quiet	A_p <10	0.988	0.236	0.982	0.094
Moderate	10< A_p <50	0.977	0.300	0.980	0.151
Active	50< A_p	0.969	0.467	0.977	0.408

Table 3.14: Averaged CC and RMS values for the selected days of CHAMP and GRACE missions for different levels of solar activity. *All RMS values are given in 10^{-12} kg/m^3*

Solar Flux	Index	CHAMP		GRACE	
		Avg CC	Avg RMS	Avg CC	Avg RMS
Low	$F_{10.7}$<75	0.989	0.130	0.989	0.081
Moderate	75< $F_{10.7}$<150	0.978	0.306	0.979	0.177
Elevated	150< $F_{10.7}$<190	0.979	0.319	0.980	0.312
High	190< $F_{10.7}$	0.961	0.506	0.983	0.632

Tables 3.13 and 3.14 show the averaged CC and RMS values for selected days of the CHAMP and GRACE missions for different periods of solar and geomagnetic activity. The averaged values are similar to the values obtained for individual days for each different level of solar and geomagnetic activity. For both CHAMP and GRACE

the values are better correlated at low and moderate periods of solar and geomagnetic activity than the high, elevated, and active periods.

3.3 Comparison of POE Derived Density to Sutton and Bruinsma Accelerometer Derived Densities for the CHAMP and GRACE Satellites

Section 3.2 showed the correlation and precision between Sutton and Bruinsma accelerometer derived densities by finding the CC and RMS values for a given set of days. In this section the CC and RMS values are found separately for POE density estimates with the Sutton and Bruinsma accelerometer densities. Later the CC and RMS values obtained for both cases are compared to check the difference between those values. The average CC and RMS values between the POE densities and the Bruinsma and Sutton accelerometer densities are found for various atmospheric models and half-life combinations. In Ref [21] the work has already been done to find the correlation between the POE density values and the Bruinsma accelerometer derived densities for the CHAMP satellite. Here the correlations between POE densities and Sutton accelerometer derived densities are shown for both the CHAMP and GRACE satellites.

3.3.1 CC and RMS Values for the CHAMP Satellite

Table 3.15: Average CC and RMS Values between Bruinsma Derived Accelerometer Densities and POE Density Estimates of CHAMP for Quiet Geomagnetic Activity Period. ***All RMS values are given in 10^{-12} kg/m^3***

Half Life Combinations Density/ballistic Coefficient (min)	CIRA - 1972		Jacchia - 1971		Jacchia - Roberts		MSISE - 1990		NRLMSISE-2000	
	CC	RMS	CC	RMS	CC	RMS	CC	RMS	CC	RMS
1.8 – 1.8	0.955	0.312	0.954	0.316	0.954	0.316	0.945	0.477	0.946	0.445
1.8 – 18	0.954	0.453	0.953	0.457	0.953	0.454	0.943	0.512	0.944	0.504
1.8 – 180	0.953	0.455	0.953	0.458	0.952	0.458	0.942	0.523	0.943	0.517
18 – 1.8	0.958	0.311	0.957	0.342	0.957	0.347	0.945	0.456	0.946	0.444
18 – 18	0.952	0.438	0.952	0.453	0.952	0.434	0.939	0.461	0.940	0.452
18 – 180	0.951	0.456	0.950	0.457	0.950	0.458	0.935	0.498	0.934	0.452
180 – 1.8	0.959	0.309	0.958	0.312	0.958	0.313	0.944	0.452	0.946	0.438
180 – 18	0.951	0.341	0.950	0.378	0.951	0.372	0.945	0.513	0.946	0.509
180 - 180	0.942	0.546	0.941	0.558	0.941	0.559	0.938	0.589	0.938	0.512

Table 3.16: Average CC and RMS values between Sutton Derived Accelerometer Densities and POE Density Estimates of CHAMP for Quiet Geomagnetic Activity Period. ***All RMS values are given in 10^{-12} kg/m^3***

Half Life Combinations Density/Ballistic Coefficient (min)	CIRA - 1972		Jacchia - 1971		Jacchia - Roberts		MSISE - 1990		NRLMSISE-2000	
	CC	RMS	CC	RMS	CC	RMS	CC	RMS	CC	RMS
1.8 – 1.8	0.954	0.312	0.954	0.316	0.954	0.316	0.945	0.477	0.946	0.445
1.8 – 18	0.954	0.453	0.953	0.457	0.953	0.454	0.943	0.512	0.944	0.504
1.8 – 180	0.953	0.455	0.953	0.458	0.952	0.458	0.942	0.523	0.943	0.517
18 – 1.8	0.958	0.311	0.957	0.342	0.957	0.347	0.945	0.456	0.946	0.444
18 – 18	0.953	0.438	0.952	0.453	0.953	0.434	0.939	0.560	0.940	0.512
18 – 180	0.951	0.456	0.950	0.457	0.950	0.458	0.935	0.498	0.934	0.452
180 – 1.8	0.959	0.309	0.958	0.312	0.958	0.313	0.944	0.452	0.946	0.438
180 – 18	0.951	0.341	0.950	0.378	0.951	0.372	0.945	0.513	0.946	0.509
180 - 180	0.942	0.546	0.941	0.558	0.941	0.559	0.938	0.589	0.938	0.512

Table 3.17: Average CC and RMS Values between Bruinsma Derived Accelerometer Densities and POE Density Estimates of CHAMP for Moderate Geomagnetic Activity Period. ***All RMS values are given in 10^{-12} kg/m^3***

Half Life Combinations Density/ballistic Coefficient (min)	CIRA - 1972		Jacchia - 1971		Jacchia - Roberts		MSISE - 1990		NRLMSISE-2000	
	CC	RMS	CC	RMS	CC	RMS	CC	RMS	CC	RMS
1.8 – 1.8	0.927	0.486	0.926	0.489	0.926	0.488	0.919	0.527	0.919	0.524
1.8 – 18	0.926	0.487	0.925	0.487	0.925	0.487	0.918	0.537	0.918	0.532
1.8 – 180	0.919	0.491	0.918	0.498	0.918	0.498	0.918	0.564	0.919	0.561
18 – 1.8	0.937	0.417	0.936	0.419	0.936	0.418	0.921	0.489	0.923	0.482
18 – 18	0.937	0.456	0.936	0.459	0.936	0.459	0.917	0.512	0.918	0.507
18 – 180	0.928	0.501	0.928	0.509	0.928	0.510	0.913	0.527	0.915	0.527
180 – 1.8	0.939	0.312	0.938	0.317	0.938	0.318	0.927	0.414	0.929	0.414
180 – 18	0.923	0.393	0.922	0.393	0.923	0.393	0.917	0.523	0.918	0.518
180 - 180	0.920	0.434	0.919	0.439	0.919	0.438	0.901	0.536	0.902	0.527

Table 3.18: Average CC and RMS Values between Sutton Derived Accelerometer Densities and POE Density Estimates of CHAMP for Moderate Geomagnetic Activity Period. ***All RMS values are given in 10^{-12} kg/m^3***

Half Life Combinations Density/Ballistic Coefficient (min)	CIRA - 1972		Jacchia - 1971		Jacchia - Roberts		MSISE - 1990		NRLMSISE-2000	
	CC	RMS	CC	RMS	CC	RMS	CC	RMS	CC	RMS
1.8 – 1.8	0.927	0.486	0.926	0.487	0.926	0.488	0.919	0.527	0.919	0.524
1.8 – 18	0.925	0.487	0.925	0.487	0.925	0.487	0.918	0.537	0.918	0.532
1.8 – 180	0.919	0.491	0.918	0.498	0.918	0.498	0.918	0.564	0.919	0.563
18 – 1.8	0.937	0.417	0.936	0.419	0.936	0.418	0.921	0.489	0.923	0.482
18 – 18	0.937	0.456	0.936	0.459	0.936	0.458	0.917	0.512	0.918	0.507
18 – 180	0.928	0.501	0.928	0.509	0.928	0.510	0.913	0.527	0.915	0.526
180 – 1.8	0.939	0.312	0.938	0.317	0.938	0.318	0.927	0.414	0.929	0.414
180 – 18	0.923	0.393	0.922	0.393	0.923	0.393	0.917	0.523	0.918	0.518
180 - 180	0.919	0.434	0.919	0.439	0.919	0.438	0.900	0.536	0.902	0.529

Table 3.19 : Average CC and RMS Values between Bruinsma Derived Accelerometer Densities and POE Density Estimates of CHAMP for Active Geomagnetic Activity Period. ***All RMS values are given in 10^{-12} kg/m^3***

Half Life Combinations Density/ballistic Coefficient (min)	CIRA - 1972		Jacchia - 1971		Jacchia - Roberts		MSISE - 1990		NRLMSISE-2000	
	CC	RMS	CC	RMS	CC	RMS	CC	RMS	CC	RMS
1.8 – 1.8	0.857	0.687	0.857	0.689	0.857	0.689	0.839	0.698	0.840	0.695
1.8 – 18	0.853	0.689	0.852	0.690	0.853	0.692	0.824	0.701	0.826	0.694
1.8 – 180	0.852	0.692	0.851	0.693	0.852	0.697	0.821	0.705	0.821	0.698
18 – 1.8	0.862	0.666	0.861	0.669	0.861	0.671	0.859	0.652	0.860	0.645
18 – 18	0.855	0.679	0.855	0.679	0.855	0.681	0.831	0.657	0.831	0.656
18 – 180	0.854	0.681	0.853	0.684	0.853	0.684	0.828	0.661	0.828	0.660
180 – 1.8	0.861	0.667	0.860	0.668	0.861	0.690	0.855	0.653	0.856	0.652
180 – 18	0.853	0.675	0.853	0.678	0.853	0.678	0.842	0.659	0.843	0.651
180 - 180	0.851	0.678	0.850	0.679	0.850	0.683	0.839	0.662	0.841	0.658

Table 3.20: Average CC and RMS Values between Sutton Derived Accelerometer Densities and POE Density Estimates of CHAMP for Active Geomagnetic Activity Period. ***All RMS values are given in 10^{-12} kg/m^3***

Half Life Combinations Density/Ballistic Coefficient (min)	CIRA - 1972		Jacchia - 1971		Jacchia - Roberts		MSISE - 1990		NRLMSISE-2000	
	CC	RMS	CC	RMS	CC	RMS	CC	RMS	CC	RMS
1.8 – 1.8	0.857	0.687	0.857	0.689	0.857	0.689	0.839	0.698	0.840	0.695
1.8 – 18	0.853	0.689	0.852	0.690	0.853	0.692	0.824	0.701	0.826	0.698
1.8 – 180	0.851	0.692	0.851	0.693	0.851	0.697	0.821	0.705	0.821	0.698
18 – 1.8	0.862	0.666	0.861	0.669	0.861	0.671	0.859	0.652	0.860	0.645
18 – 18	0.855	0.679	0.855	0.679	0.855	0.681	0.831	0.657	0.831	0.656
18 – 180	0.854	0.681	0.853	0.684	0.853	0.684	0.828	0.661	0.828	0.660
180 – 1.8	0.861	0.667	0.860	0.668	0.861	0.690	0.855	0.653	0.856	0.652
180 – 18	0.853	0.675	0.853	0.678	0.853	0.678	0.843	0.657	0.843	0.651
180 - 180	0.851	0.678	0.850	0.679	0.850	0.683	0.839	0.662	0.841	0.658

Table 3.21 : Average CC and RMS Values between Bruinsma Derived Accelerometer Densities and POE Density Estimates of CHAMP for Low Solar Activity Period. ***All RMS values are given in 10^{-12} kg/m^3***

Half Life Combinations Density/ballistic Coefficient (min)	CIRA - 1972		Jacchia - 1971		Jacchia - Roberts		MSISE - 1990		NRLMSISE-2000	
	CC	RMS	CC	RMS	CC	RMS	CC	RMS	CC	RMS
1.8 – 1.8	0.944	0.213	0.944	0.213	0.943	0.216	0.939	0.285	0.939	0.285
1.8 – 18	0.942	0.222	0.941	0.224	0.942	0.226	0.932	0.298	0.933	0.298
1.8 – 180	0.941	0.231	0.941	0.234	0.941	0.232	0.931	0.300	0.931	0.300
18 – 1.8	0.956	0.206	0.956	0.207	0.955	0.207	0.942	0.274	0.943	0.272
18 – 18	0.943	0.217	0.943	0.218	0.943	0.219	0.936	0.289	0.936	0.286
18 – 180	0.942	0.229	0.941	0.229	0.942	0.229	0.935	0.292	0.935	0.291
180 – 1.8	0.959	0.199	0.959	0.201	0.959	0.202	0.946	0.271	0.946	0.270
180 – 18	0.942	0.208	0.942	0.209	0.941	0.209	0.941	0.278	0.941	0.274
180 - 180	0.939	0.211	0.939	0.213	0.938	0.216	0.934	0.283	0.936	0.279

Table 3.22: Average CC and RMS Values between Sutton Derived Accelerometer Densities and POE Density Estimates of CHAMP for Low Solar Activity Period. ***All RMS values are given in 10^{-12} kg/m^3***

Half Life Combinations Density/Ballistic Coefficient (min)	CIRA - 1972		Jacchia - 1971		Jacchia - Roberts		MSISE - 1990		NRLMSISE-2000	
	CC	RMS	CC	RMS	CC	RMS	CC	RMS	CC	RMS
1.8 – 1.8	0.945	0.213	0.944	0.213	0.943	0.216	0.939	0.285	0.939	0.285
1.8 – 18	0.942	0.222	0.941	0.224	0.942	0.226	0.932	0.298	0.933	0.298
1.8 – 180	0.941	0.231	0.941	0.234	0.941	0.232	0.931	0.299	0.931	0.296
18 – 1.8	0.956	0.206	0.956	0.206	0.955	0.207	0.943	0.274	0.943	0.272
18 – 18	0.943	0.217	0.944	0.218	0.943	0.219	0.936	0.289	0.936	0.286
18 – 180	0.942	0.229	0.941	0.229	0.942	0.229	0.935	0.292	0.935	0.291
180 – 1.8	0.959	0.199	0.959	0.201	0.959	0.202	0.946	0.271	0.946	0.270
180 – 18	0.942	0.208	0.942	0.209	0.941	0.209	0.941	0.278	0.941	0.274
180 - 180	0.939	0.211	0.938	0.213	0.938	0.216	0.934	0.283	0.936	0.279

Table 3.23 : Average CC and RMS Values between Bruinsma Derived Accelerometer Densities and POE Density Estimates of CHAMP for Moderate Solar Activity Period. ***All RMS values are given in 10^{-12} kg/m^3***

Half Life Combinations Density/ballistic Coefficient (min)	CIRA - 1972		Jacchia - 1971		Jacchia - Roberts		MSISE - 1990		NRLMSISE-2000	
	CC	RMS	CC	RMS	CC	RMS	CC	RMS	CC	RMS
1.8 – 1.8	0.937	0.342	0.937	0.346	0.937	0.344	0.929	0.378	0.929	0.374
1.8 – 18	0.931	0.352	0.931	0.358	0.931	0.357	0.924	0.387	0.925	0.385
1.8 – 180	0.928	0.387	0.927	0.388	0.927	0.392	0.920	0.393	0.923	0.389
18 – 1.8	0.939	0.339	0.937	0.341	0.939	0.341	0.931	0.369	0.932	0.368
18 – 18	0.936	0.343	0.936	0.345	0.936	0.344	0.928	0.372	0.928	0.366
18 – 180	0.933	0.368	0.932	0.368	0.932	0.371	0.922	0.381	0.923	0.380
180 – 1.8	0.941	0.324	0.941	0.328	0.940	0.327	0.935	0.359	0.935	0.357
180 – 18	0.935	0.336	0.934	0.336	0.935	0.337	0.923	0.360	0.926	0.359
180 - 180	0.934	0.359	0.933	0.362	0.933	0.363	0.919	0.377	0.921	0.363

Table 3.24: Average CC and RMS Values between Sutton Derived Accelerometer Densities and POE Density Estimates of CHAMP for Moderate Solar Activity Period. ***All RMS values are given in 10^{-12} kg/m^3***

Half Life Combinations Density/Ballistic Coefficient (min)	CIRA - 1972		Jacchia - 1971		Jacchia - Roberts		MSISE - 1990		NRLMSISE-2000	
	CC	RMS	CC	RMS	CC	RMS	CC	RMS	CC	RMS
1.8 – 1.8	0.937	0.342	0.937	0.346	0.937	0.345	0.929	0.378	0.929	0.374
1.8 – 18	0.931	0.351	0.931	0.358	0.931	0.357	0.924	0.387	0.925	0.384
1.8 – 180	0.928	0.387	0.927	0.388	0.927	0.392	0.920	0.393	0.923	0.389
18 – 1.8	0.938	0.339	0.937	0.341	0.939	0.341	0.931	0.369	0.932	0.368
18 – 18	0.936	0.342	0.937	0.345	0.936	0.344	0.928	0.372	0.928	0.366
18 – 180	0.933	0.368	0.932	0.368	0.933	0.371	0.922	0.381	0.923	0.380
180 – 1.8	0.941	0.324	0.941	0.328	0.940	0.327	0.935	0.359	0.935	0.357
180 – 18	0.934	0.336	0.935	0.337	0.935	0.337	0.922	0.360	0.926	0.357
180 - 180	0.934	0.359	0.933	0.362	0.933	0.363	0.919	0.377	0.920	0.363

Table 3.25 : Average CC and RMS Values between Bruinsma Derived Accelerometer Densities and POE Density Estimates of CHAMP for Elevated Solar Activity Period. ***All RMS values are given in 10^{-12} kg/m^3***

Half Life Combinations Density/ballistic Coefficient (min)	CIRA - 1972		Jacchia - 1971		Jacchia - Roberts		MSISE - 1990		NRLMSISE-2000	
	CC	RMS	CC	RMS	CC	RMS	CC	RMS	CC	RMS
1.8 – 1.8	0.911	0.542	0.911	0.546	0.910	0.544	0.901	0.556	0.901	0.552
1.8 – 18	0.909	0.578	0.907	0.586	0.908	0.588	0.898	0.598	0.899	0.592
1.8 – 180	0.907	0.610	0.906	0.625	0.906	0.627	0.895	0.659	0.898	0.647
18 – 1.8	0.928	0.534	0.928	0.538	0.928	0.537	0.919	0.542	0.920	0.543
18 – 18	0.927	0.541	0.927	0.556	0.926	0.557	0.916	0.556	0.917	0.555
18 – 180	0.921	0.558	0.920	0.561	0.920	0.559	0.909	0.588	0.911	0.583
180 – 1.8	0.927	0.525	0.926	0.525	0.926	0.525	0.913	0.549	0.913	0.535
180 – 18	0.916	0.532	0.915	0.533	0.916	0.536	0.910	0.595	0.911	0.593
180 - 180	0.914	0.533	0.913	0.535	0.913	0.537	0.900	0.607	0.901	0.598

Table 3.26: Average CC and RMS Values between Sutton Derived Accelerometer Densities and POE Density Estimates of CHAMP for Elevated Solar Activity Period. ***All RMS values are given in 10^{-12} kg/m^3***

Half Life Combinations Density/Ballistic Coefficient (min)	CIRA - 1972		Jacchia - 1971		Jacchia - Roberts		MSISE - 1990		NRLMSISE-2000	
	CC	RMS	CC	RMS	CC	RMS	CC	RMS	CC	RMS
1.8 – 1.8	0.911	0.542	0.910	0.546	0.910	0.544	0.901	0.556	0.901	0.552
1.8 – 18	0.909	0.578	0.907	0.586	0.908	0.588	0.898	0.598	0.899	0.592
1.8 – 180	0.907	0.610	0.906	0.625	0.906	0.627	0.895	0.659	0.898	0.648
18 – 1.8	0.928	0.534	0.928	0.538	0.928	0.537	0.919	0.542	0.920	0.543
18 – 18	0.927	0.541	0.927	0.556	0.926	0.557	0.916	0.556	0.917	0.555
18 – 180	0.921	0.558	0.920	0.561	0.920	0.559	0.909	0.588	0.911	0.583
180 – 1.8	0.927	0.525	0.926	0.525	0.926	0.525	0.912	0.549	0.913	0.535
180 – 18	0.916	0.532	0.915	0.533	0.916	0.536	0.910	0.595	0.911	0.593
180 - 180	0.915	0.533	0.913	0.535	0.914	0.537	0.900	0.607	0.901	0.599

Table 3.27 : Average CC and RMS Values between Bruinsma Derived Accelerometer Densities and POE Density Estimates of CHAMP for High Solar Activity Period. ***All RMS values are given in 10^{-12} kg/m^3***

Half Life Combinations Density/ballistic Coefficient (min)	CIRA - 1972		Jacchia - 1971		Jacchia - Roberts		MSISE - 1990		NRLMSISE-2000	
	CC	RMS	CC	RMS	CC	RMS	CC	RMS	CC	RMS
1.8 – 1.8	0.903	0.873	0.902	0.873	0.900	0.879	0.888	0.884	0.899	0.884
1.8 – 18	0.897	0.885	0.896	0.886	0.896	0.888	0.884	0.896	0.889	0.888
1.8 – 180	0.894	0.902	0.892	0.899	0.892	0.901	0.879	0.925	0.881	0.920
18 – 1.8	0.910	0.864	0.908	0.865	0.908	0.874	0.908	0.885	0.909	0.878
18 – 18	0.906	0.879	0.905	0.881	0.905	0.887	0.896	0.895	0.898	0.894
18 – 180	0.898	0.888	0.898	0.892	0.897	0.898	0.893	0.909	0.893	0.907
180 – 1.8	0.909	0.845	0.904	0.848	0.904	0.845	0.905	0.889	0.906	0.884
180 – 18	0.905	0.865	0.905	0.875	0.904	0.873	0.892	0.899	0.894	0.889
180 - 180	0.897	0.872	0.895	0.874	0.895	0.879	0.891	0.904	0.893	0.900

Table 3.28: Average CC and RMS Values between Sutton Derived Accelerometer Densities and POE Density Estimates of CHAMP for High Solar Activity Period. ***All RMS values are given in 10^{-12} kg/m^3***

Half Life Combinations Density/Ballistic Coefficient (min)	CIRA - 1972		Jacchia - 1971		Jacchia - Roberts		MSISE - 1990		NRLMSISE-2000	
	CC	RMS	CC	RMS	CC	RMS	CC	RMS	CC	RMS
1.8 – 1.8	0.903	0.873	0.902	0.873	0.903	0.879	0.888	0.884	0.899	0.887
1.8 – 18	0.897	0.885	0.896	0.886	0.896	0.888	0.884	0.896	0.889	0.888
1.8 – 180	0.894	0.901	0.892	0.899	0.892	0.901	0.879	0.925	0.881	0.920
18 – 1.8	0.910	0.864	0.908	0.865	0.908	0.874	0.908	0.885	0.909	0.878
18 – 18	0.906	0.879	0.905	0.881	0.905	0.887	0.896	0.895	0.898	0.894
18 – 180	0.898	0.888	0.898	0.892	0.897	0.898	0.893	0.909	0.893	0.907
180 – 1.8	0.909	0.844	0.904	0.848	0.904	0.845	0.905	0.889	0.906	0.884
180 – 18	0.906	0.865	0.905	0.875	0.904	0.873	0.892	0.899	0.895	0.889
180 - 180	0.897	0.872	0.895	0.874	0.896	0.879	0.891	0.904	0.893	0.901

3.3.2 Summary of the Comparison of POE Derived Density to Sutton and Bruinsma Accelerometer Derived Densities for CHAMP

Tables 3.15 to 3.30 show the CC and RMS values between the POE density estimates and the Sutton and Bruinsma accelerometer densities for CHAMP. The Sutton and Bruinsma accelerometer densities have similar CC and RMS values with the POE density estimates. This indicates that the Sutton accelerometer densities are similar to the Bruinsma densities for CHAMP satellite. The CC and RMS values for the Jacchia family models are similar with the CIRA-72 model performing the best. The CC and RMS values for the MSIS family models are also similar with the NRLMSISE-00 model performing the best. The Jacchia family models have better CC and RMS values than the MSIS family models.

The density and ballistic half-life combinations of 180-1.8 min and 18-1.8 min yielded the best CC and RMS values for all solar and geomagnetic activity levels. Also, the CC and RMS values were better for the days with low and moderate solar and geomagnetic days than for the active and high days. The CC values ranged around 0.89-0.95 and RMS values around $0.1\text{-}0.9 \times 10^{-12}$ kg/m^3 for all levels of solar and geomagnetic activity. Hence, the Sutton and Bruinsma accelerometer densities are proven to be similar based on these CC and RMS values for CHAMP.

3.3.3 CC and RMS values for the GRACE Satellite

Table 3.29 : Average CC and RMS Values between Bruinsma Derived Accelerometer Densities and POE Density Estimates of GRACE for Quiet Geomagnetic Activity Period. ***All RMS values are given in 10^{-12} kg/m^3***

Half Life Combinations Density/ballistic Coefficient (min)	CIRA - 1972		Jacchia - 1971		Jacchia - Roberts		MSISE - 1990		NRLMSISE-2000	
	CC	RMS	CC	RMS	CC	RMS	CC	RMS	CC	RMS
1.8 – 1.8	0.954	0.177	0.952	0.179	0.951	0.181	0.944	0.199	0.948	0.199
1.8 – 18	0.951	0.181	0.951	0.183	0.952	0.185	0.941	0.201	0.945	0.200
1.8 – 180	0.950	0.198	0.950	0.199	0.951	0.203	0.933	0.203	0.937	0.200
18 – 1.8	0.958	0.171	0.957	0.176	0.958	0.181	0.946	0.195	0.948	0.191
18 – 18	0.949	0.176	0.949	0.176	0.945	0.189	0.941	0.206	0.945	0.201
18 – 180	0.948	0.187	0.947	0.189	0.941	0.189	0.935	0.208	0.941	0.207
180 – 1.8	0.959	0.169	0.957	0.171	0.956	0.187	0.948	0.193	0.951	0.189
180 – 18	0.942	0.184	0.941	0.193	0.941	0.198	0.937	0.201	0.938	0.195
180 - 180	0.933	0.187	0.932	0.188	0.932	0.199	0.938	0.202	0.939	0.199

Table 3.30: Average CC and RMS Values between Sutton Derived Accelerometer Densities and POE Density Estimates of GRACE for Quiet Geomagnetic Activity Period. ***All RMS values are given in 10^{-12} kg/m^3***

Half Life Combinations Density/Ballistic Coefficient (min)	CIRA - 1972		Jacchia - 1971		Jacchia - Roberts		MSISE - 1990		NRLMSISE-2000	
	CC	RMS	CC	RMS	CC	RMS	CC	RMS	CC	RMS
1.8 – 1.8	0.954	0.177	0.952	0.179	0.951	0.181	0.943	0.199	0.948	0.199
1.8 – 18	0.951	0.181	0.951	0.183	0.952	0.185	0.941	0.201	0.945	0.200
1.8 – 180	0.951	0.198	0.950	0.199	0.951	0.203	0.933	0.203	0.937	0.200
18 – 1.8	0.958	0.171	0.957	0.176	0.958	0.181	0.943	0.195	0.947	0.191
18 – 18	0.949	0.176	0.948	0.176	0.945	0.189	0.941	0.206	0.945	0.201
18 – 180	0.947	0.187	0.947	0.189	0.941	0.189	0.935	0.208	0.941	0.206
180 – 1.8	0.959	0.169	0.957	0.171	0.956	0.187	0.948	0.193	0.951	0.189
180 – 18	0.942	0.183	0.941	0.193	0.940	0.198	0.937	0.201	0.939	0.195
180 - 180	0.933	0.187	0.932	0.188	0.932	0.199	0.938	0.202	0.939	0.199

Table 3.31 : Average CC and RMS Values between Bruinsma Derived Accelerometer Densities and POE Density Estimates of GRACE for Moderate Geomagnetic Activity Period. ***All RMS values are given in 10^{-12} kg/m^3***

Half Life Combinations Density/ballistic Coefficient (min)	CIRA - 1972		Jacchia - 1971		Jacchia - Roberts		MSISE - 1990		NRLMSISE-2000	
	CC	RMS	CC	RMS	CC	RMS	CC	RMS	CC	RMS
1.8 – 1.8	0.911	0.216	0.909	0.219	0.908	0.219	0.901	0.277	0.902	0.277
1.8 – 18	0.906	0.219	0.905	0.220	0.905	0.220	0.899	0.278	0.901	0.277
1.8 – 180	0.905	0.221	0.905	0.226	0.904	0.224	0.898	0.281	0.899	0.281
18 – 1.8	0.918	0.212	0.918	0.213	0.917	0.214	0.910	0.269	0.912	0.267
18 – 18	0.914	0.217	0.912	0.217	0.912	0.218	0.903	0.273	0.906	0.272
18 – 180	0.913	0.219	0.911	0.219	0.911	0.221	0.900	0.276	0.906	0.274
180 – 1.8	0.928	0.201	0.927	0.203	0.927	0.205	0.917	0.265	0.919	0.264
180 – 18	0.924	0.209	0.921	0.210	0.922	0.211	0.916	0.263	0.916	0.262
180 - 180	0.918	0.216	0.917	0.216	0.916	0.219	0.911	0.256	0.913	0.254

Table 3.32: Average CC and RMS Values between Sutton Derived Accelerometer Densities and POE Density Estimates of GRACE for Moderate Geomagnetic Activity Period. ***All RMS values are given in 10^{-12} kg/m^3***

Half Life Combinations Density/Ballistic Coefficient (min)	CIRA - 1972		Jacchia - 1971		Jacchia - Roberts		MSISE - 1990		NRLMSISE-2000	
	CC	RMS	CC	RMS	CC	RMS	CC	RMS	CC	RMS
1.8 – 1.8	0.910	0.216	0.909	0.219	0.908	0.219	0.901	0.277	0.902	0.277
1.8 – 18	0.906	0.219	0.906	0.220	0.905	0.220	0.899	0.278	0.901	0.276
1.8 – 180	0.905	0.221	0.905	0.226	0.904	0.224	0.899	0.281	0.899	0.281
18 – 1.8	0.918	0.212	0.918	0.213	0.917	0.214	0.910	0.269	0.912	0.267
18 – 18	0.914	0.217	0.912	0.217	0.912	0.218	0.903	0.273	0.906	0.272
18 – 180	0.912	0.219	0.911	0.219	0.911	0.221	0.900	0.276	0.906	0.274
180 – 1.8	0.928	0.201	0.927	0.203	0.927	0.205	0.917	0.265	0.919	0.264
180 – 18	0.924	0.209	0.921	0.210	0.922	0.211	0.916	0.263	0.916	0.262
180 - 180	0.918	0.216	0.918	0.216	0.916	0.219	0.911	0.256	0.913	0.253

Table 3.33 : Average CC and RMS Values between Bruinsma Derived Accelerometer Densities and POE Density Estimates of GRACE for Active Geomagnetic Activity Period. ***All RMS values are given in 10^{-12} kg/m^3***

Half Life Combinations Density/ballistic Coefficient (min)	CIRA - 1972		Jacchia - 1971		Jacchia - Roberts		MSISE - 1990		NRLMSISE-2000	
	CC	RMS	CC	RMS	CC	RMS	CC	RMS	CC	RMS
1.8 – 1.8	0.887	0.477	0.886	0.479	0.886	0.479	0.863	0.484	0.865	0.482
1.8 – 18	0.882	0.479	0.882	0.482	0.881	0.482	0.852	0.488	0.863	0.486
1.8 – 180	0.879	0.481	0.878	0.483	0.878	0.483	0.851	0.495	0.862	0.494
18 – 1.8	0.891	0.475	0.889	0.478	0.890	0.478	0.873	0.479	0.874	0.477
18 – 18	0.885	0.476	0.884	0.479	0.885	0.479	0.869	0.481	0.876	0.477
18 – 180	0.882	0.478	0.881	0.479	0.880	0.482	0.867	0.485	0.869	0.479
180 – 1.8	0.904	0.467	0.904	0.470	0.904	0.470	0.881	0.473	0.879	0.471
180 – 18	0.893	0.471	0.892	0.474	0.891	0.478	0.878	0.475	0.881	0.474
180 - 180	0.892	0.474	0.891	0.479	0.890	0.483	0.872	0.483	0.872	0.479

Table 3.34: Average CC and RMS Values between Sutton Derived Accelerometer Densities and POE Density Estimates of GRACE for Active Geomagnetic Activity Period. ***All RMS values are given in 10^{-12} kg/m^3***

Half Life Combinations Density/Ballistic Coefficient (min)	CIRA - 1972		Jacchia - 1971		Jacchia - Roberts		MSISE - 1990		NRLMSISE-2000	
	CC	RMS	CC	RMS	CC	RMS	CC	RMS	CC	RMS
1.8 – 1.8	0.887	0.477	0.886	0.479	0.886	0.479	0.864	0.484	0.865	0.482
1.8 – 18	0.882	0.478	0.882	0.482	0.881	0.482	0.852	0.488	0.863	0.486
1.8 – 180	0.879	0.481	0.878	0.483	0.878	0.483	0.851	0.495	0.862	0.494
18 – 1.8	0.891	0.475	0.889	0.478	0.890	0.478	0.874	0.479	0.874	0.477
18 – 18	0.885	0.476	0.884	0.479	0.885	0.479	0.869	0.481	0.876	0.477
18 – 180	0.882	0.478	0.881	0.479	0.880	0.482	0.867	0.485	0.869	0.479
180 – 1.8	0.904	0.467	0.904	0.470	0.904	0.470	0.881	0.473	0.879	0.471
180 – 18	0.893	0.471	0.892	0.474	0.893	0.477	0.878	0.475	0.881	0.474
180 - 180	0.893	0.474	0.891	0.479	0.890	0.483	0.872	0.482	0.872	0.479

Table 3.35 : Average CC and RMS Values between Bruinsma Derived Accelerometer Densities and POE Density Estimates of GRACE for Low Solar Activity Period. ***All RMS values are given in 10^{-12} kg/m^3***

Half Life Combinations Density/ballistic Coefficient (min)	CIRA - 1972		Jacchia - 1971		Jacchia - Roberts		MSISE - 1990		NRLMSISE-2000	
	CC	RMS	CC	RMS	CC	RMS	CC	RMS	CC	RMS
1.8 – 1.8	0.952	0.203	0.951	0.203	0.951	0.203	0.949	0.265	0.950	0.265
1.8 – 18	0.951	0.208	0.950	0.207	0.951	0.209	0.946	0.273	0.948	0.272
1.8 – 180	0.949	0.212	0.948	0.218	0.948	0.222	0.943	0.280	0.943	0.280
18 – 1.8	0.956	0.185	0.955	0.188	0.955	0.187	0.952	0.254	0.954	0.253
18 – 18	0.953	0.197	0.952	0.199	0.952	0.198	0.948	0.245	0.949	0.244
18 – 180	0.947	0.201	0.946	0.202	0.945	0.206	0.944	0.242	0.945	0.242
180 – 1.8	0.961	0.179	0.960	0.182	0.960	0.185	0.956	0.251	0.959	0.249
180 – 18	0.957	0.182	0.956	0.184	0.956	0.184	0.952	0.258	0.953	0.257
180 - 180	0.954	0.191	0.953	0.194	0.952	0.194	0.947	0.263	0.948	0.256

Table 3.36: Average CC and RMS Values between Sutton Derived Accelerometer Densities and POE Density Estimates of GRACE for Low Solar Activity Period. ***All RMS values are given in 10^{-12} kg/m^3***

Half Life Combinations Density/Ballistic Coefficient (min)	CIRA - 1972		Jacchia - 1971		Jacchia - Roberts		MSISE - 1990		NRLMSISE-2000	
	CC	RMS	CC	RMS	CC	RMS	CC	RMS	CC	RMS
1.8 – 1.8	0.953	0.203	0.951	0.203	0.951	0.204	0.949	0.265	0.950	0.265
1.8 – 18	0.951	0.208	0.950	0.207	0.951	0.209	0.946	0.273	0.949	0.272
1.8 – 180	0.949	0.212	0.948	0.218	0.948	0.222	0.943	0.280	0.943	0.280
18 – 1.8	0.956	0.185	0.955	0.188	0.955	0.188	0.952	0.254	0.954	0.253
18 – 18	0.953	0.197	0.951	0.199	0.952	0.198	0.948	0.245	0.949	0.244
18 – 180	0.947	0.201	0.946	0.202	0.945	0.206	0.944	0.242	0.945	0.242
180 – 1.8	0.961	0.179	0.960	0.182	0.960	0.185	0.955	0.251	0.959	0.249
180 – 18	0.957	0.181	0.956	0.184	0.956	0.184	0.952	0.258	0.953	0.257
180 - 180	0.954	0.191	0.953	0.194	0.952	0.194	0.947	0.263	0.948	0.256

Table 3.37 : Average CC and RMS Values between Bruinsma Derived Accelerometer Densities and POE Density Estimates of GRACE for Moderate Solar Activity Period. ***All RMS values are given in 10^{-12} kg/m^3***

Half Life Combinations Density/ballistic Coefficient (min)	CIRA - 1972		Jacchia - 1971		Jacchia - Roberts		MSISE - 1990		NRLMSISE-2000	
	CC	RMS	CC	RMS	CC	RMS	CC	RMS	CC	RMS
1.8 – 1.8	0.937	0.341	0.936	0.342	0.936	0.344	0.919	0.368	0.921	0.363
1.8 – 18	0.935	0.352	0.935	0.355	0.934	0.354	0.913	0.375	0.917	0.368
1.8 – 180	0.931	0.354	0.931	0.353	0.930	0.353	0.908	0.383	0.911	0.374
18 – 1.8	0.942	0.336	0.941	0.338	0.942	0.338	0.931	0.359	0.933	0.358
18 – 18	0.938	0.338	0.937	0.339	0.936	0.339	0.928	0.353	0.928	0.359
18 – 180	0.933	0.343	0.932	0.344	0.932	0.346	0.925	0.351	0.926	0.363
180 – 1.8	0.948	0.314	0.947	0.318	0.948	0.317	0.940	0.349	0.941	0.344
180 – 18	0.944	0.326	0.944	0.326	0.944	0.327	0.933	0.350	0.934	0.349
180 - 180	0.941	0.334	0.940	0.337	0.939	0.338	0.931	0.352	0.935	0.351

Table 3.38: Average CC and RMS Values between Sutton Derived Accelerometer Densities and POE Density Estimates of GRACE for Moderate Solar Activity Period. ***All RMS values are given in 10^{-12} kg/m^3***

Half Life Combinations Density/Ballistic Coefficient (min)	CIRA - 1972		Jacchia - 1971		Jacchia - Roberts		MSISE - 1990		NRLMSISE-2000	
	CC	RMS	CC	RMS	CC	RMS	CC	RMS	CC	RMS
1.8 – 1.8	0.937	0.341	0.936	0.342	0.936	0.344	0.919	0.368	0.921	0.363
1.8 – 18	0.936	0.352	0.935	0.355	0.934	0.354	0.913	0.375	0.917	0.368
1.8 – 180	0.931	0.354	0.931	0.353	0.930	0.353	0.908	0.383	0.911	0.374
18 – 1.8	0.942	0.335	0.941	0.338	0.942	0.338	0.931	0.359	0.933	0.358
18 – 18	0.938	0.338	0.937	0.339	0.936	0.339	0.928	0.353	0.928	0.359
18 – 180	0.933	0.343	0.931	0.344	0.932	0.346	0.925	0.351	0.926	0.363
180 – 1.8	0.949	0.314	0.947	0.318	0.948	0.317	0.940	0.349	0.941	0.344
180 – 18	0.944	0.326	0.944	0.326	0.944	0.327	0.933	0.350	0.934	0.349
180 - 180	0.941	0.334	0.940	0.337	0.939	0.338	0.931	0.352	0.937	0.351

3.3.4 Summary of the Comparison of POE Derived Density to Sutton and Bruinsma Accelerometer Derived Densities for GRACE

Tables 3.31 to 3.38 show the CC and RMS values between the POE density estimates and the Bruinsma and Sutton accelerometer densities for GRACE. The CC and RMS values between the POE density estimates and Bruinsma densities and Sutton densities are nearly the same for all solar and geomagnetic activity levels considered and also for all different combinations of density and BC correlated half-lives. However, the correlation worsened slightly with increase in the intensity of geomagnetic activity level. GRACE doesn't have any POE data available for high and elevated solar activity levels.

The Jacchia family POE density estimates showed better correlation when compared with the MSIS family POE density estimates. Among the Jacchia family models, the CIRA-72 POE density estimates showed better correlation with the accelerometer densities than the Jacchia-71 and Jacchia-Roberts POE density estimates. For the MSIS family models, the NRLMSISE-00 POE density estimates correlated better with the accelerometer densities than the MSISE-90 POE density estimates. POE density estimates from the Jacchia family of models were proven to have better correlation with the accelerometer densities than those from the MSIS family.

The POE density estimates correlated well with Bruinsma and Sutton accelerometer densities for higher density half-life of 180 min and for lower BC half-life of 1.8 min. The POE density estimates of atmospheric models with density and

ballistic coefficient correlated half life combinations of 180-1.8 min showed the best correlation. Hence, the Sutton and Bruinsma accelerometer densities are proven to be similar based on the CC and RMS values for GRACE.

3.4 Conclusion

The purpose of this chapter is to determine the proximity between Bruinsma and Sutton densities derived from the accelerometers on board the CHAMP and GRACE satellites. The correlation between these two densities was found by calculating the CC values and the precision between these two sets of densities was found by determining the RMS values. The CC values indicate a high correlation between both the sets of values, while the RMS values showed higher degree of precision at low and moderate periods of solar and geomagnetic activity than the periods of active and high geomagnetic and solar activity.

The CIRA-72 POE densities from the Jacchia family of atmospheric models and the NRLMSISE-00 POE densities from the MSIS family of models proved to have better correlation with the Sutton and Bruinsma densities. Also, the POE density estimates obtained using density and ballistic coefficient correlated half life combinations of 18-1.8 min, and 180-1.8 min showed the best correlation with accelerometer densities. The overall CC and RMS results obtained proved the high level of proximity between the Sutton and Bruinsma accelerometer derived densities. Therefore, Sutton accelerometer derived densities can be considered for use as a substitute for Bruinsma accelerometer derived densities in future work.

4. Examination of POE Density Estimates for ICESat and TerraSAR-X

This chapter examines the POE density estimates obtained using CIRA-72, and NRLMSISE-00 as baseline density models for the CHAMP, GRACE, ICESat, and TerraSAR-X satellites. The main purpose of this chapter is to study the behavior of POE density estimates from the ICESat and TerraSAR-X satellites by comparing them with the POE density estimates from the CHAMP and GRACE satellites, which possess accelerometers on board. Unlike CHAMP and GRACE, the ICESat and TerraSAR-X satellites do not carry on-board accelerometers, so finding the correlation of POE density estimates with accelerometer densities is not possible in the case of ICESat and TerraSAR-X. Therefore, the POE density estimates for all four satellites are plotted and the variations in density estimates are studied from those plots. By observing trends in the plots, the behavior and variation of POE density estimates from the ICESat and TerraSAR-X satellites are studied and checked to see whether they follow a similar trend as the CHAMP and GRACE satellites. Also, the POE density estimates are compared with the values from the Jacchia-71 empirical model. Ref [20], [21], [25] and [49] are used as references for the work done on CHAMP and GRACE in this chapter.

The estimated POE densities are examined for various Solar and Geomagnetic activity levels, various density and ballistic coefficient correlated half-lives, and both CIRA-72 and NRLMSISE-00 as baseline models. The POE densities are estimated for all combinations of 1.8 min, 18 min, and 180 min of density and ballistic

coefficient half-lives. The subsequent sections in this chapter show and explain the variations in plots for each different case and describe the observed variation.

4.1 Examination of POE Density Estimates for different periods of Solar and Geomagnetic Activity

This section describes the variation in POE estimated densities for various levels of solar and geomagnetic activity. The comparison plots are observed to study the variation in density estimates obtained from the atmospheric models CIRA-72, and NRLMSISE-00.

4.1.1 Low Solar and Quiet Geomagnetic Activity

The days of low solar activity coupled with quiet geomagnetic activity do not cause much variation in the atmospheric density. From the year 2001 to 2008, a total of fifteen days with low solar activity ($F_{10.7}$<75) and quiet geomagnetic activity (Ap<10) were selected and POE density estimates were obtained using the CIRA-72, NRLMSISE-00 models along with the densities from Jacchia-71 model.

Table 4.1: Selected Days with Low Solar and Quiet Geomagnetic Activity.

Year	Month	Day	A_p	$F_{10.7}$
2005	Oct	28	5	73.1
2005	Oct	29	3	74.1
2006	Oct	26	2	71.9
2007	Apr	08	3	71.1
2007	Oct	09	1	68.7
2007	Oct	28	7	67.5
2007	Nov	02	2	67.9
2007	Nov	04	4	67.7
2008	Feb	20	6	70.9
2008	Feb	25	4	71.4
2008	Mar	02	9	69.2
2008	Mar	16	6	70.3
2008	Mar	20	8	68.4
2008	Oct	05	4	67.4
2008	Oct	17	2	70

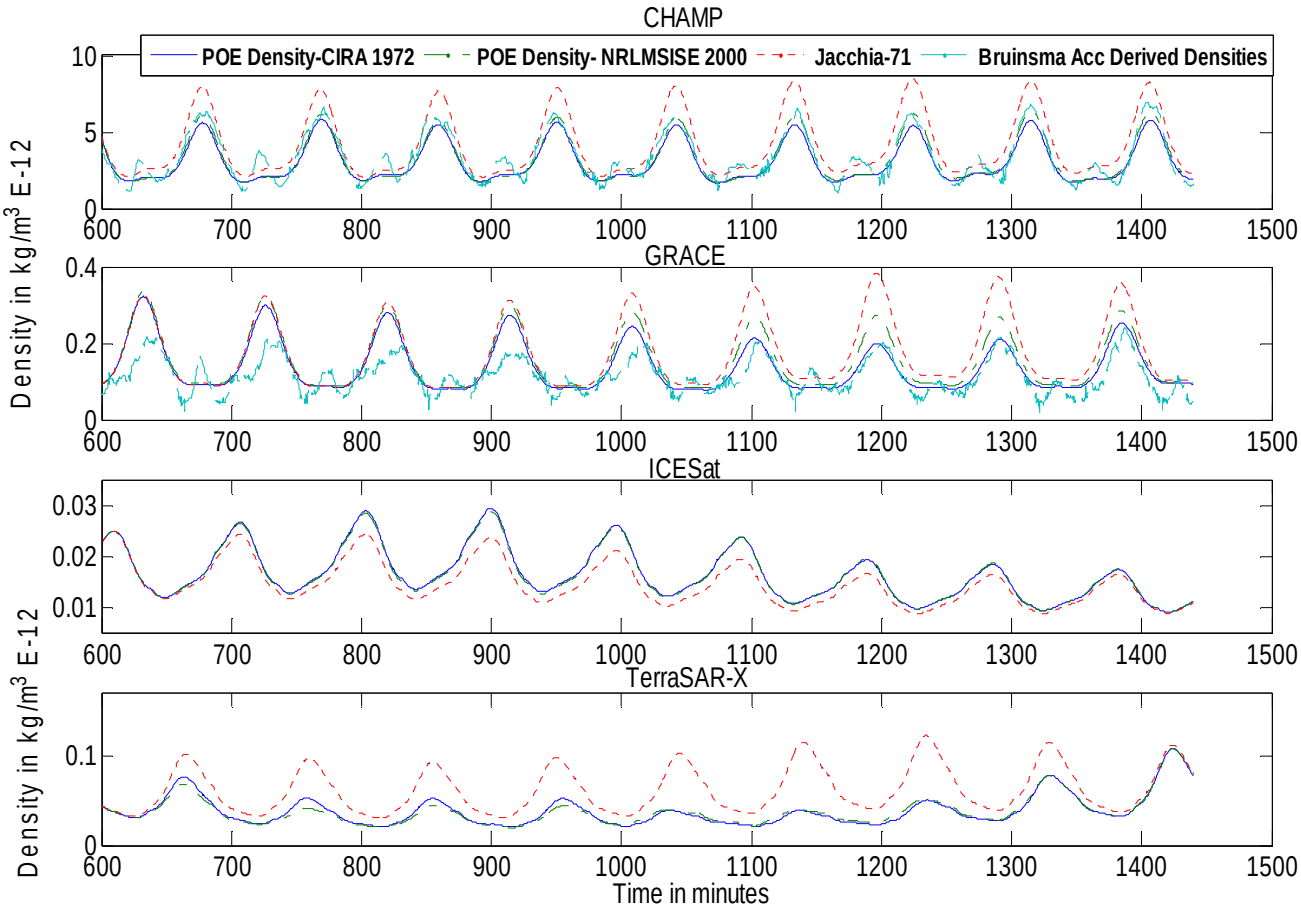

Figure 4.1 POE density estimates of CHAMP, GRACE, ICESat and TerraSAR-X on October 17, 2008.

Fig 4.1 shows the variation in POE density estimates for October 17, 2008, which is chosen as a representative day for the fifteen days examined with low solar and quiet geomagnetic activity. All fifteen days selected showed results similar to Fig 4.1. The plots of the CHAMP and GRACE satellites show that the CIRA-72 POE density estimates correlate better with the accelerometer densities than the NRLMSISE-00 POE density estimates. Accelerometer densities correlated worst with the Jacchia-71 model densities thus showing the difference between actual model density values and

the corrected model density values estimated using POE data. The Jacchia-71 model densities are higher than POE density estimates for all satellites except ICESat, where it is low. This difference may be either due to the source of ICESat POE data obtained, which is different from the source of CHAMP, GRACE, and TerraSAR-X POE data or it could be due to the difference in the ICESat orbit and geometry. The ICESat and TerraSAR-X showed variations in POE density estimates similar to CHAMP and GRACE for days of low solar and quiet geomagnetic activity.

4.1.2 Moderate Geomagnetic Activity

Moderate Geomagnetic Activity corresponds to the days having Ap index where 10<Ap<50. The variation in atmospheric density is expected to be somewhat higher for the moderate period than for quiet geomagnetic activity. A total of ten days from the years 2001-2008 with moderate geomagnetic activity were selected and POE density estimates were obtained for those days.

Table 4.2: Selected Days with Moderate Geomagnetic Activity

Year	Month	Day	A_p
2004	Mar	01	21
2005	Jun	04	22
2006	Nov	25	15
2007	Apr	01	29
2007	Oct	03	12
2007	Oct	18	17
2008	Feb	28	23
2008	Mar	09	30
2008	Mar	14	16
2008	Oct	11	34

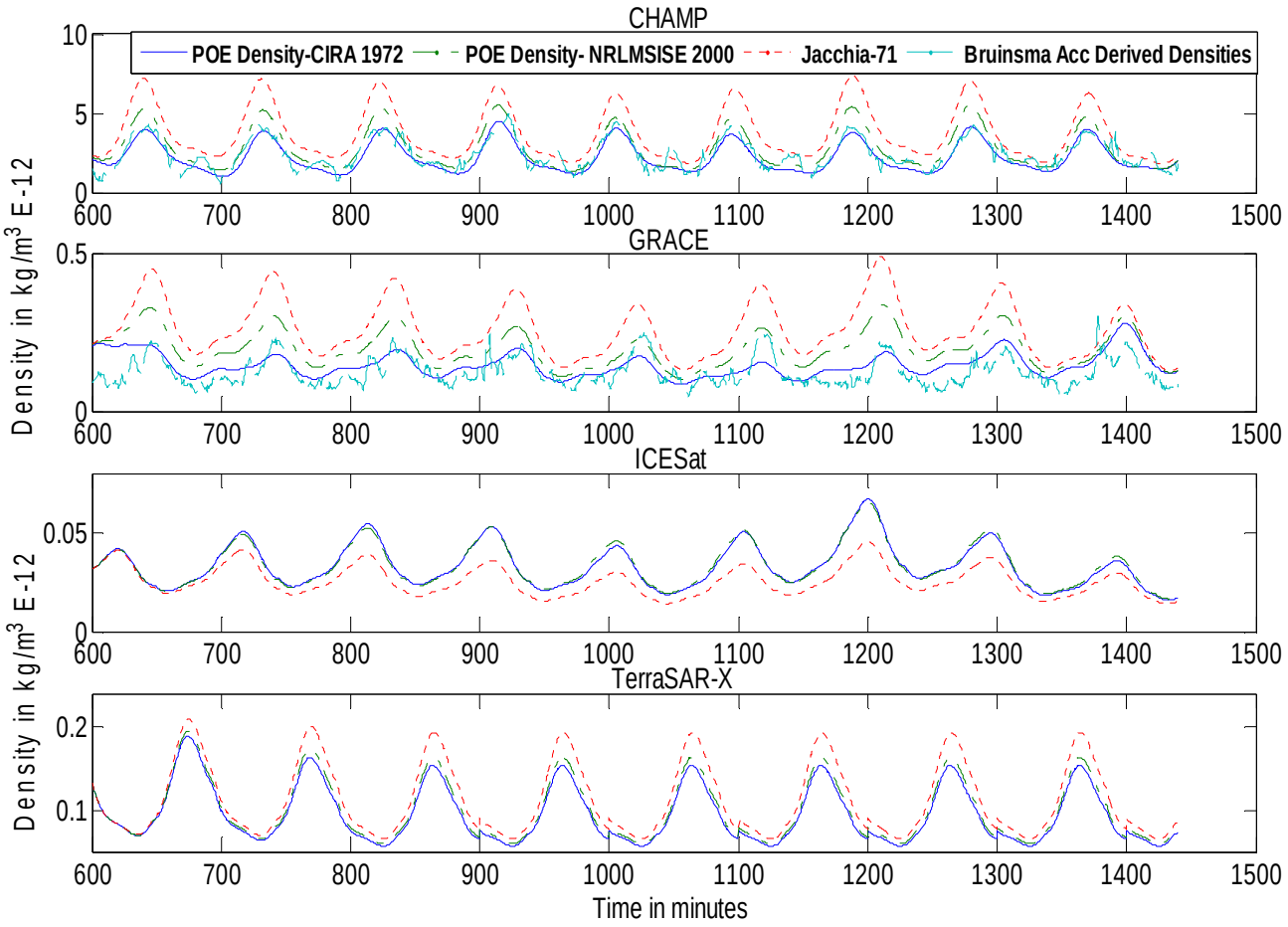

Figure 4.2 POE density estimates of CHAMP, GRACE, ICESat and TerraSAR-X on October 3, 2007

Fig 4.2 shows the variation in POE density estimates for October 3, 2007, which is chosen as a representative day for all ten days examined with moderate geomagnetic activity. All ten days selected showed results similar to Fig 4.2. Similar to the case of quiet geomagnetic activity, the CIRA-72 POE density estimates correlate better with the accelerometer densities for the CHAMP and GRACE satellites. For all four

satellites, the NRLMSISE-00 POE density estimates are higher in value than the CIRA-72 POE density estimates. The Jacchia-71 model densities are again higher than POE density estimates for CHAMP, GRACE, and TerraSAR-X satellites and are lower for ICESat. The overall correlation between density values worsened slightly for days with moderate geomagnetic activity when compared with days of quiet geomagnetic activity. ICESat, CHAMP, GRACE, and TerraSAR-X showed similar trends in the variation of POE density estimates for moderate geomagnetic activity.

4.1.3 Active Geomagnetic Activity

The days having A_p index more than 50 (A_p>50) are the days of Active Geomagnetic activity. The atmospheric density varies highly during the periods of active geomagnetic activity. Five days with active geomagnetic activity from the years 2001 to 2008 are selected and POE density estimates are obtained for those days. Very few days experienced active geomagnetic activity from the year 2001 to 2008. TerraSAR-X operational life does not have any days with active geomagnetic activity.

Table 4.3: Selected Days with Active Geomagnetic Activity

Year	Month	Day	A_p
2003	Nov	11	61
2003	Nov	13	52
2004	Nov	08	140
2005	May	30	90
2005	Jun	12	54

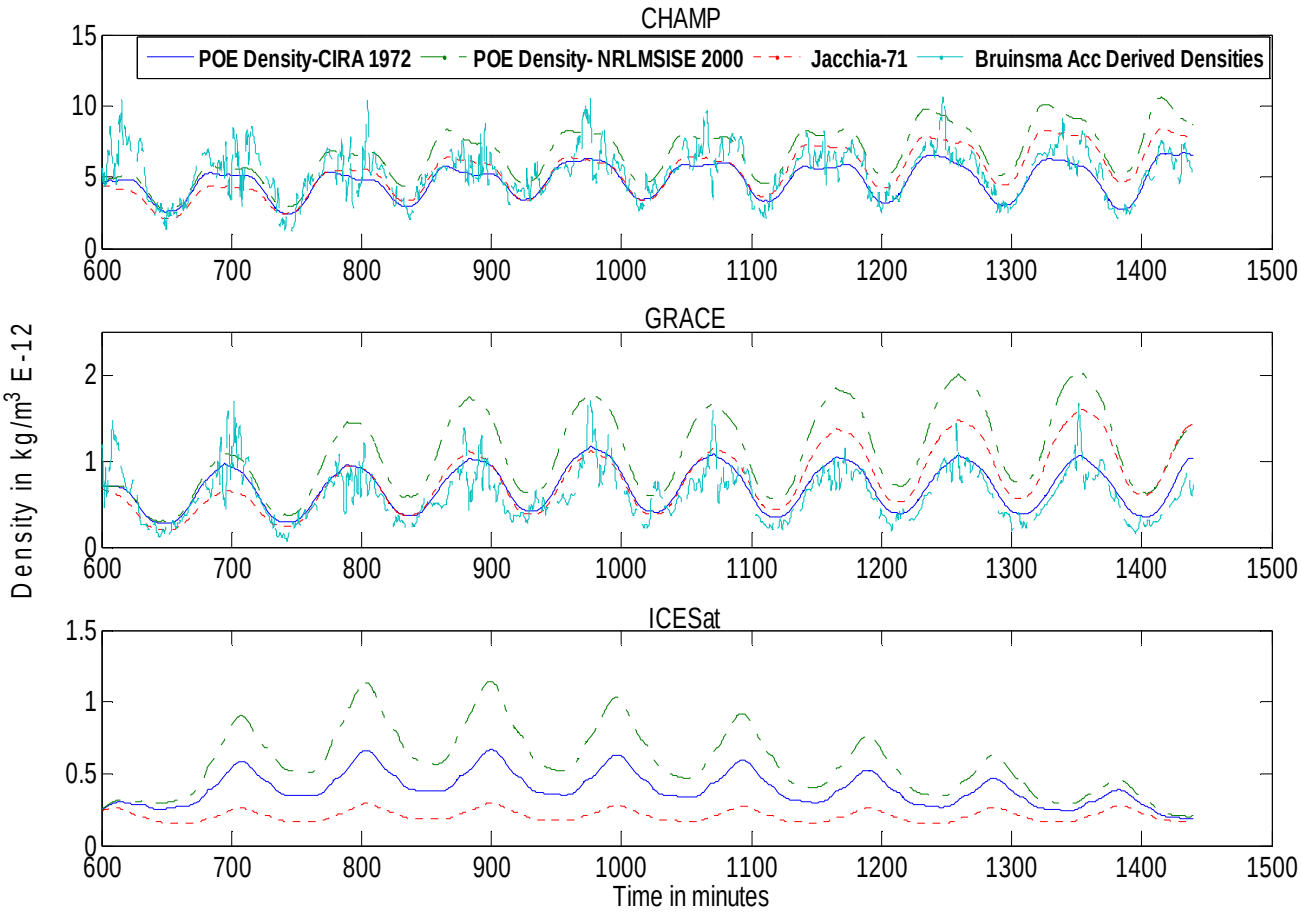

Figure 4.3 POE density estimates of CHAMP, GRACE, ICESat and TerraSAR-X on May 30, 2005

Fig 4.3 shows the variation in POE density estimates for May 30, 2005, which is chosen as a representative day for the five days examined with active geomagnetic activity. All five days selected showed results similar to Fig 4.3. The CIRA-72 POE density estimates correlate well with the accelerometer densities for the CHAMP and GRACE satellites. The accelerometer densities are observed to be highly variable.

The NRLMSISE-00 POE density estimates are higher than the CIRA-72 POE density estimates for all three satellites. In the case of CHAMP and GRACE, the Jacchia-71 model densities are lower than NRLMSISE-00 POE density estimates and higher than CIRA-72 POE densities, which is a different trend than observed for low and moderate geomagnetic activity periods. This different trend in the Jacchia-71 empirical model densities for CHAMP and GRACE may be due to the increase in geomagnetic activity, which results in higher atmospheric density. For ICESat the NRLMSISE-00 POE density estimates have higher values followed by the CIRA-72 POE densities and the Jacchia-71 model densities. The POE density estimates are more highly variable for active periods of geomagnetic activity than the low and moderate periods. ICESat, CHAMP, and GRACE showed similar trends in the variation of POE density estimates for active geomagnetic activity.

4.1.4 Moderate Solar Activity

The days with moderate solar activity have solar flux, $F_{10.7}$ in the range of 75-150. Ten days with moderate solar activity were selected from the years 2001 to 2008 and POE density estimates were obtained for those days. Two different days were chosen as representative days for all the fifteen days to plot the density estimates because the mission lives of ICESat and TerraSAR-X do not have common days with moderate solar activity.

Table 4.4: Selected Days with Moderate Solar Activity

Year	Month	Day	$F_{10.7}$
2003	Feb	24	102.2
2003	Oct	19	120.4
2004	Mar	01	101.8
2004	Nov	12	97.4
2005	Feb	21	94.5
2005	Jun	02	93.3
2006	Feb	28	77.1
2007	Dec	10	86.9
2008	Mar	25	88.6
2008	Jan	06	79.2

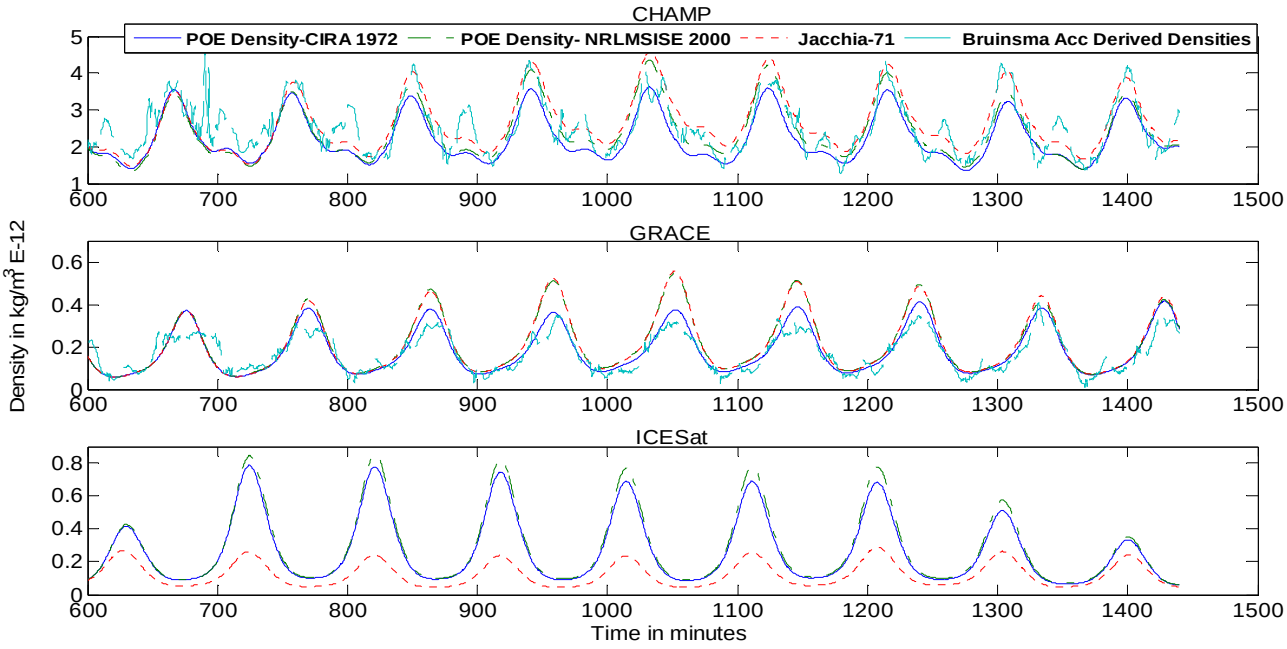

Figure 4.4 POE density estimates of CHAMP, GRACE and ICESat on February 28, 2006

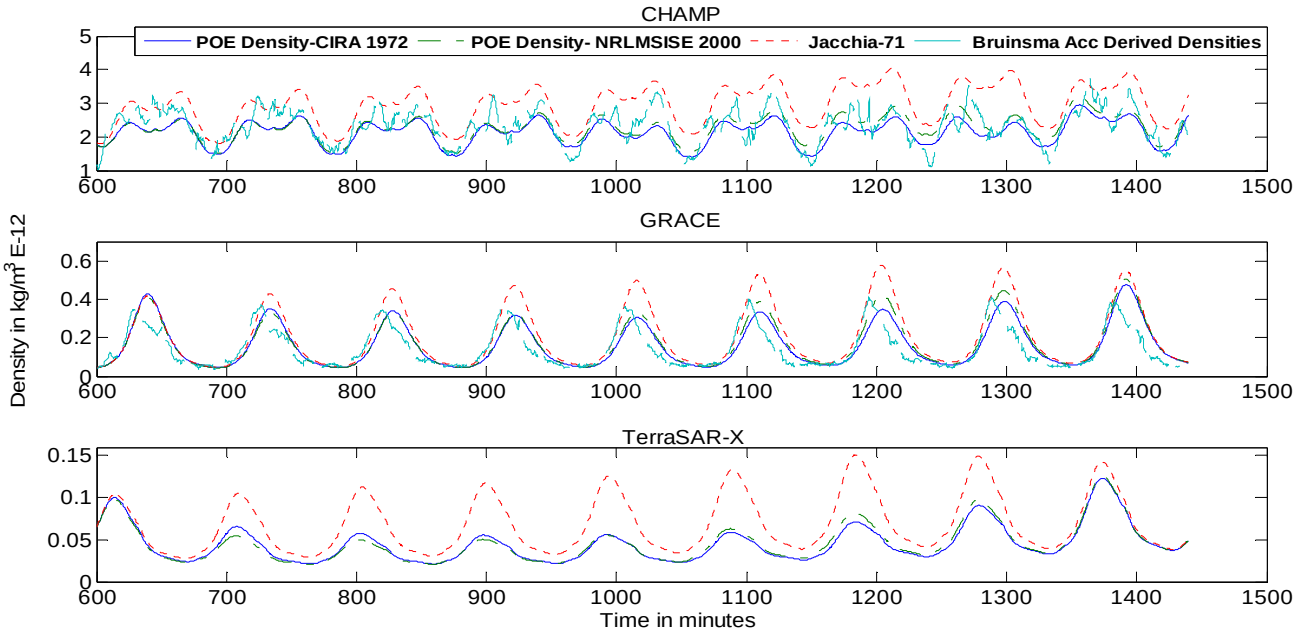

Figure 4.5 POE density estimates of CHAMP, GRACE and TerraSAR-X on March 25, 2008

Figures 4.4 and 4.5 show the variation in POE density estimates for February 28, 2006 and March 25, 2008, which are chosen as representative days for all ten days examined with moderate solar activity. All ten days selected showed results similar to Figures 4.4 and 4.5. The variation in POE density estimates for moderate solar activity is similar to low solar activity. For CHAMP and GRACE, the CIRA-72 POE density estimates correlated better with the accelerometer densities than the NRLMSISE-00 POE density estimates. However, the closeness in correlation is not as good compared to the lower solar activity period. The Jacchia-71 model densities showed the worst correlation with accelerometer densities and POE density estimates. TerraSAR-X exhibited a similar trend in the variation of densities compared to that of CHAMP and GRACE. For ICESat, the empirical Jacchia model density estimates are lower than the POE density estimates. This is opposite to the trend observed for the

CHAMP, GRACE and TerraSAR-X satellites, which are at a lower altitude than ICESat. For all four satellites, NRLMSISE-00 POE density estimates are higher than the CIRA-72 POE density estimates.

4.1.6 Elevated Solar Activity

Elevated Solar Activity represents the days having Solar Flux in the range of 150 – 190 ($150<F_{10.7}<190$). From the years 2001 to 2008, five days with elevated solar activity were selected and POE density estimates were obtained. An elevated level of solar activity causes intense variations in the atmospheric density. Since the elevated levels of solar activity do not occur very often there are only few days between 2001 - 2008 that have elevated levels of solar activity. GRACE and TerraSAR-X did not experience days of elevated solar activity in their orbital life.

Table 4.5: Selected Days with Elevated Solar Activity

Year	Month	Day	$F_{10.7}$
2003	Mar	06	150.3
2003	Mar	09	152.7
2003	Oct	21	151.5
2003	Oct	22	153.5
2003	Oct	23	183.2

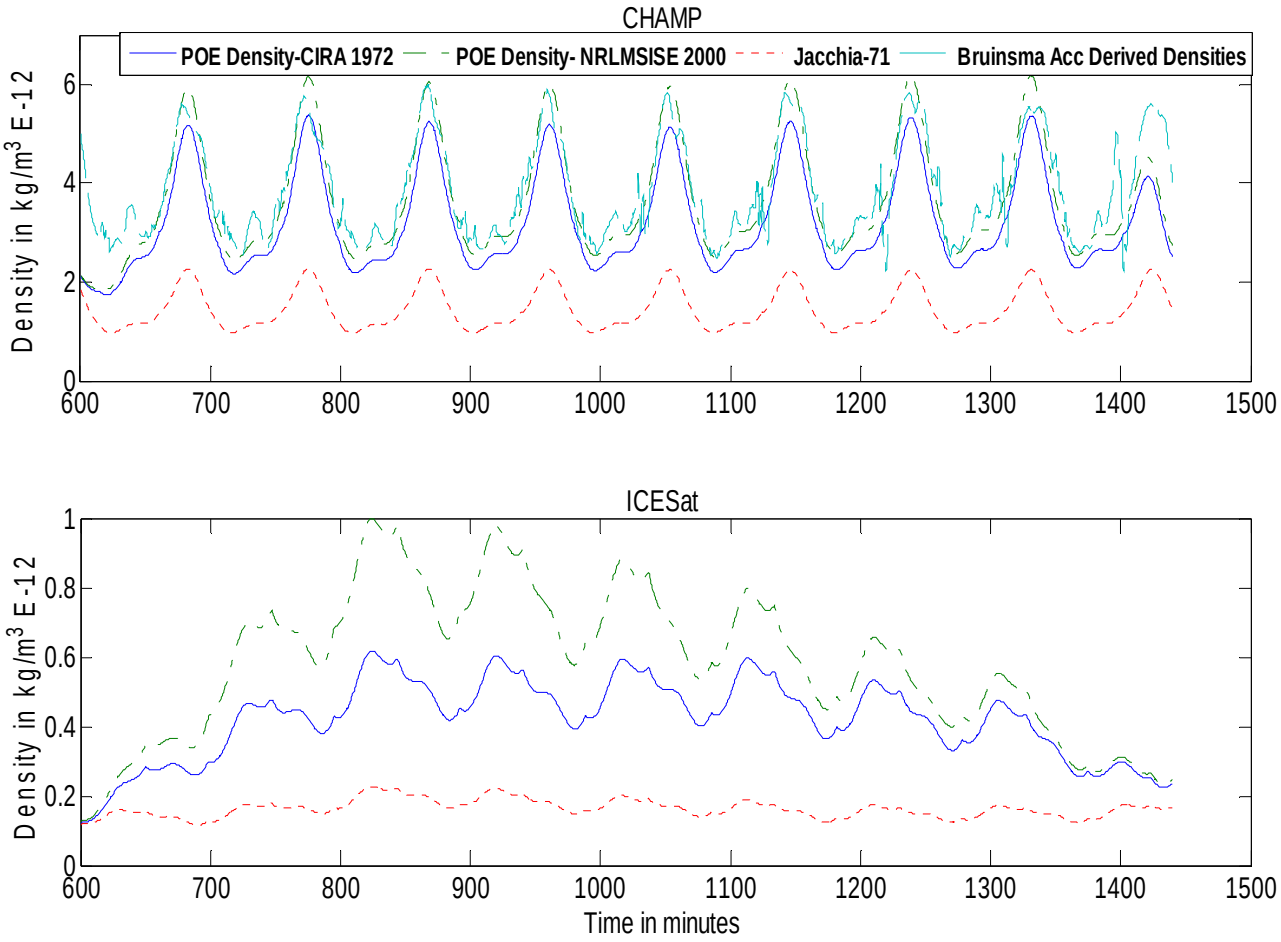

Figure 4.6 POE density estimates of CHAMP and ICESat on March 9, 2003.

Fig 4.6 shows the variation in POE density estimates for March 9, 2003, which is chosen as a representative day for all five days with elevated solar activity. All five days selected showed results similar to Fig 4.6. The density variations are high for elevated solar activity when compared to low and moderate activity. CIRA-72 POE density estimates are found to correlate better with the accelerometer densities for CHAMP. The Jacchia-71 model densities are found to be lower than the POE density

estimates. ICESat exhibits a similar trend in variation when compared to CHAMP except for large variations between the atmospheric models. The NRLMSISE-00 POE density estimates are higher than CIRA-72 POE density estimates for both CHAMP and ICESat.

4.1.7 High Solar Activity

The days with solar flux, $F_{10.}7$, greater than 190 are considered to be days of high solar activity. Very few days are found to have high levels of solar activity from the years 2001 to 2008. The POE density estimates were obtained for five days with high solar activity from the years 2001 to 2008 by generating corrections to the CIRA-72 and NRLSMISE-00 atmospheric models. Since the solar flux is very high, the density variations are highly variable. GRACE and TerraSAR-X do not have days of high solar activity in their mission life.

Table 4.6: Selected Days with High Solar Activity

Year	Month	Day	$F_{10.7}$
2003	Oct	25	221.5
2003	Oct	26	243.4
2003	Oct	27	257.2
2003	Oct	28	274.4
2003	Oct	29	279.1

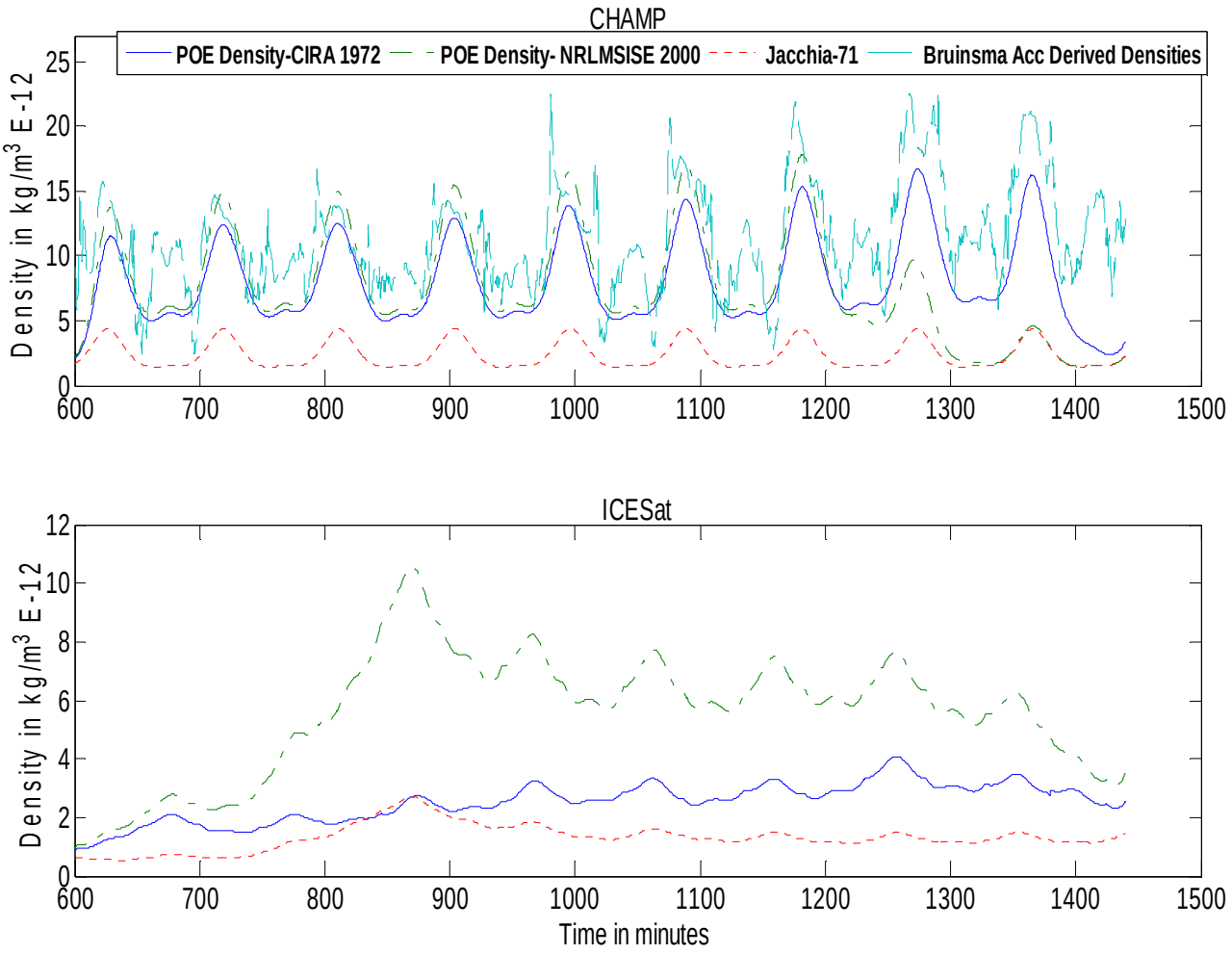

Figure 4.7 POE density estimates of CHAMP and ICESat on October 29, 2003

Fig 4.7 shows the variation in POE density estimates for October 29, 2003, which is chosen as a representative day for all five selected days with elevated solar activity. All five days selected showed results similar to Fig 4.7. The accelerometer densities for CHAMP in Figure 4.7 are highly variable. The degree of correlation between accelerometer densities and POE density estimates are found to be worse than any of the previous cases. High Solar Activity caused extreme fluctuations in atmospheric

density for this day. As usual, CIRA-72 POE density estimates showed better correlation with the accelerometer densities. The Jacchia-71 model densities are lower than POE density estimates for CHAMP and ICESat, which is different from the case of low and moderate solar activity but the same as elevated solar activity. For CHAMP, the Jacchia-71 model densities are lower than POE density estimates for elevated and high solar activity days because of the high solar intensity for these days. The NRLMSISE-00 POE density estimates are higher than the CIRA-72 POE density estimates for both CHAMP and ICESat. Overall, the density variation for ICESat is similar to that of CHAMP for high solar activity periods.

4.2 Variation in Density Correlated Half-Life

This section describes the effect of varying density correlated half-lives on POE density estimates of all four satellites. While varying the density correlated half-life the Ballistic Coefficient correlated half-life is kept constant. The density half-lives used in this section are 1.8 min, 18 min, and 180 min with BC half-life kept constant at 18 min. Plots were made separately for CIRA-72 and NRLMSISE-00 POE density estimates to study the effect for each model.

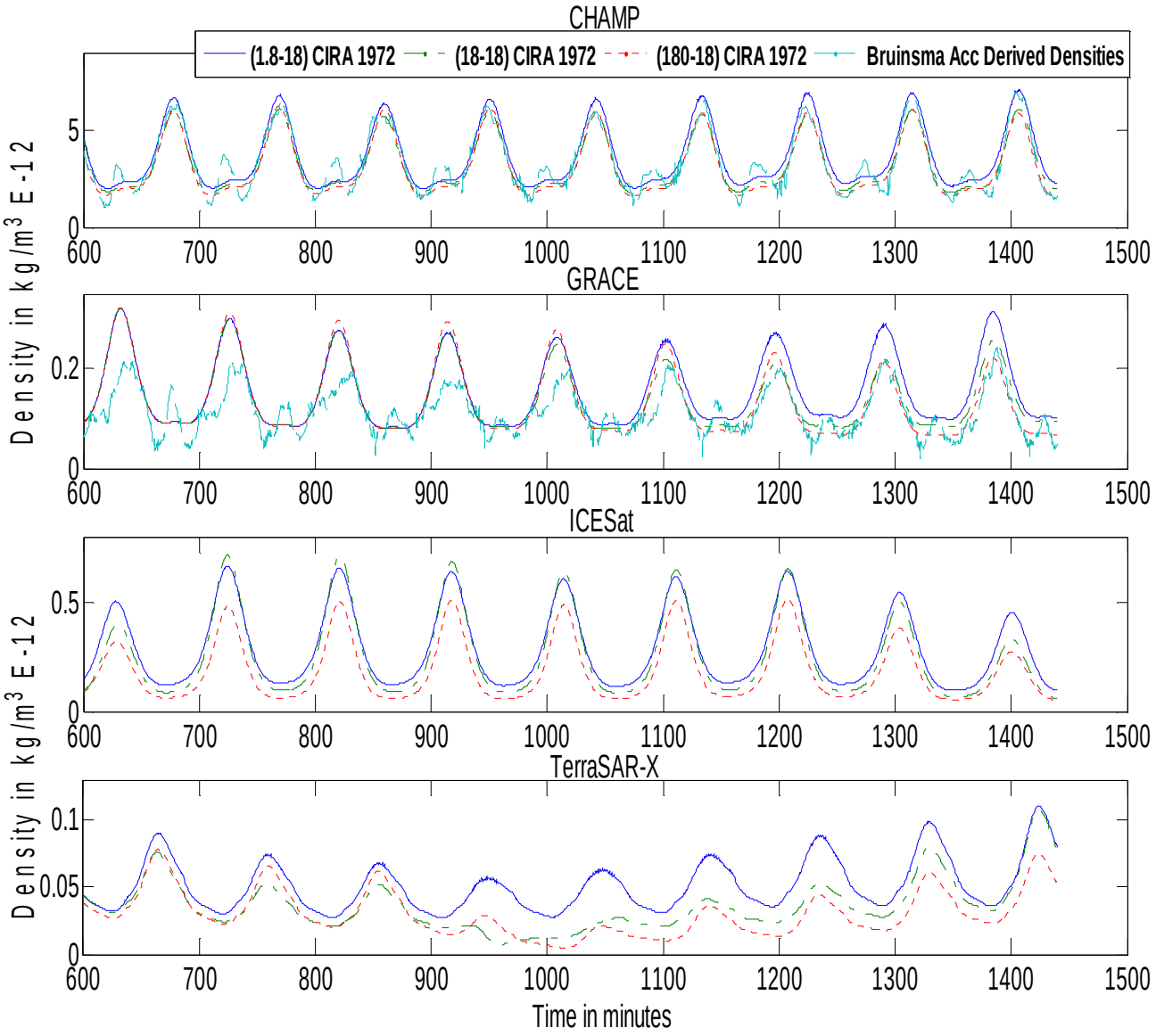

Figure 4.8 **Effect of varying density correlated half-lives on CIRA-72 POE density estimates.**

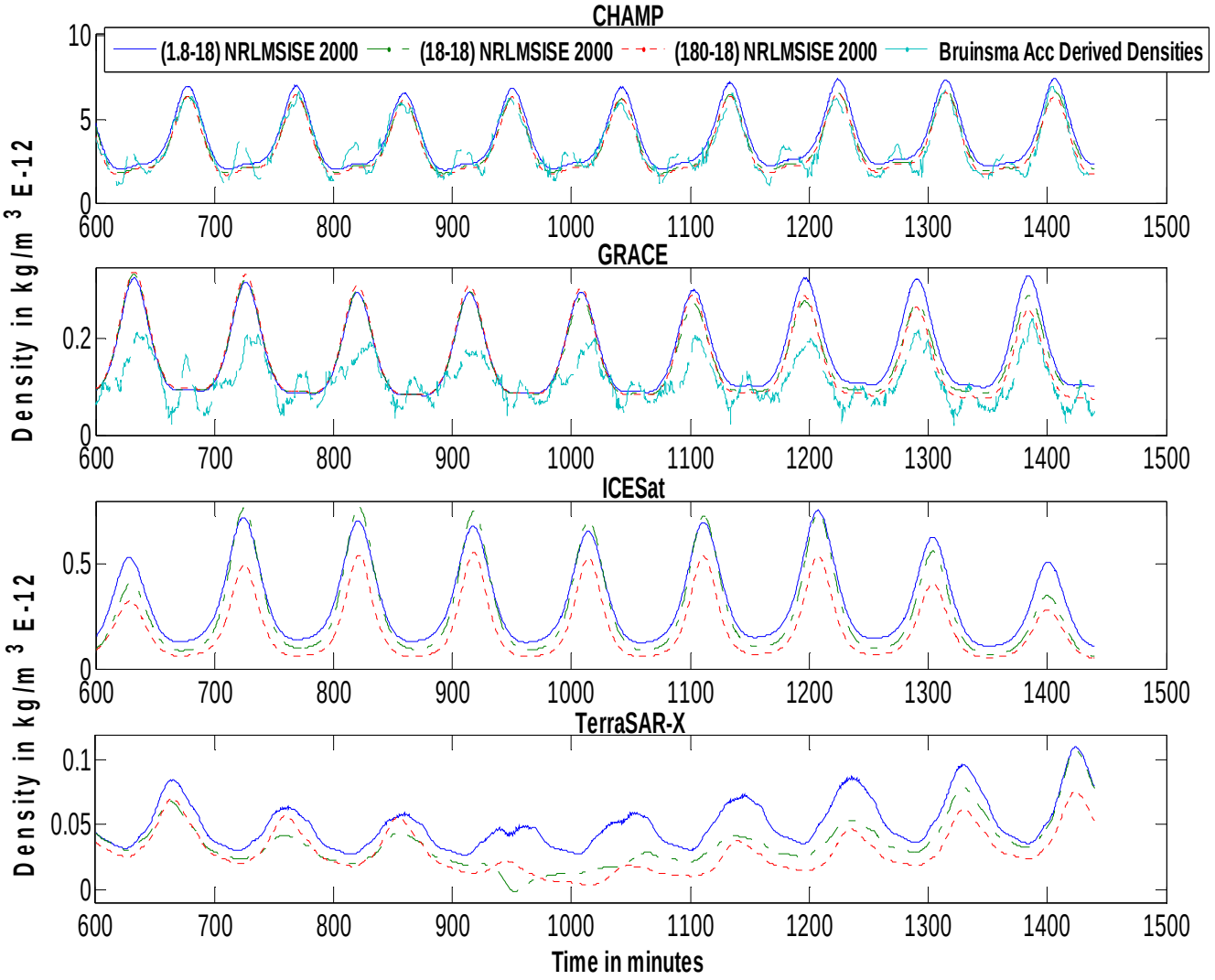

Figure 4.9 Effect of varying density correlated half-lives on NRLMSISE-00 POE density estimates.

Figures 4.8 and 4.9 show the effect of varying density correlated half-life on CIRA-72 and NRLMSISE-00 POE density estimates for a day (Oct 17, 2008) of low solar and quiet geomagnetic activity. A total of 6 days were selected with different levels of solar and geomagnetic activity and POE densities were estimated by varying both

the density and BC correlated half-lives. The results obtained by varying BC half-life are presented in the next section. All six days selected showed similar results and Oct 17, 2008 was chosen as a representative day. The POE density estimates decreased as the density correlated half-life increased. Density correlated half-life with 180 min has the lower density estimates and 1.8 min density correlated half-life has the higher density estimates. The same trend is observed for all the four satellites CHAMP, GRACE, ICESat, and TerraSAR-X and for both the atmospheric density models CIRA-72 and NRLMSISE-00. For CHAMP and GRACE, the accelerometer densities correlated better with the higher density half-lives of 18 min and 180 min.

4.3 Variation in Ballistic Coefficient Correlated Half-Life

This section describes the effect of varying ballistic coefficient correlated half-lives on POE density estimates. While varying the ballistic coefficient correlated half-life the density half-life is kept constant. The BC correlated half-lives used in this section are 1.8 min, 18 min, and 180 min with the density correlated half-life kept constant at 18 min.

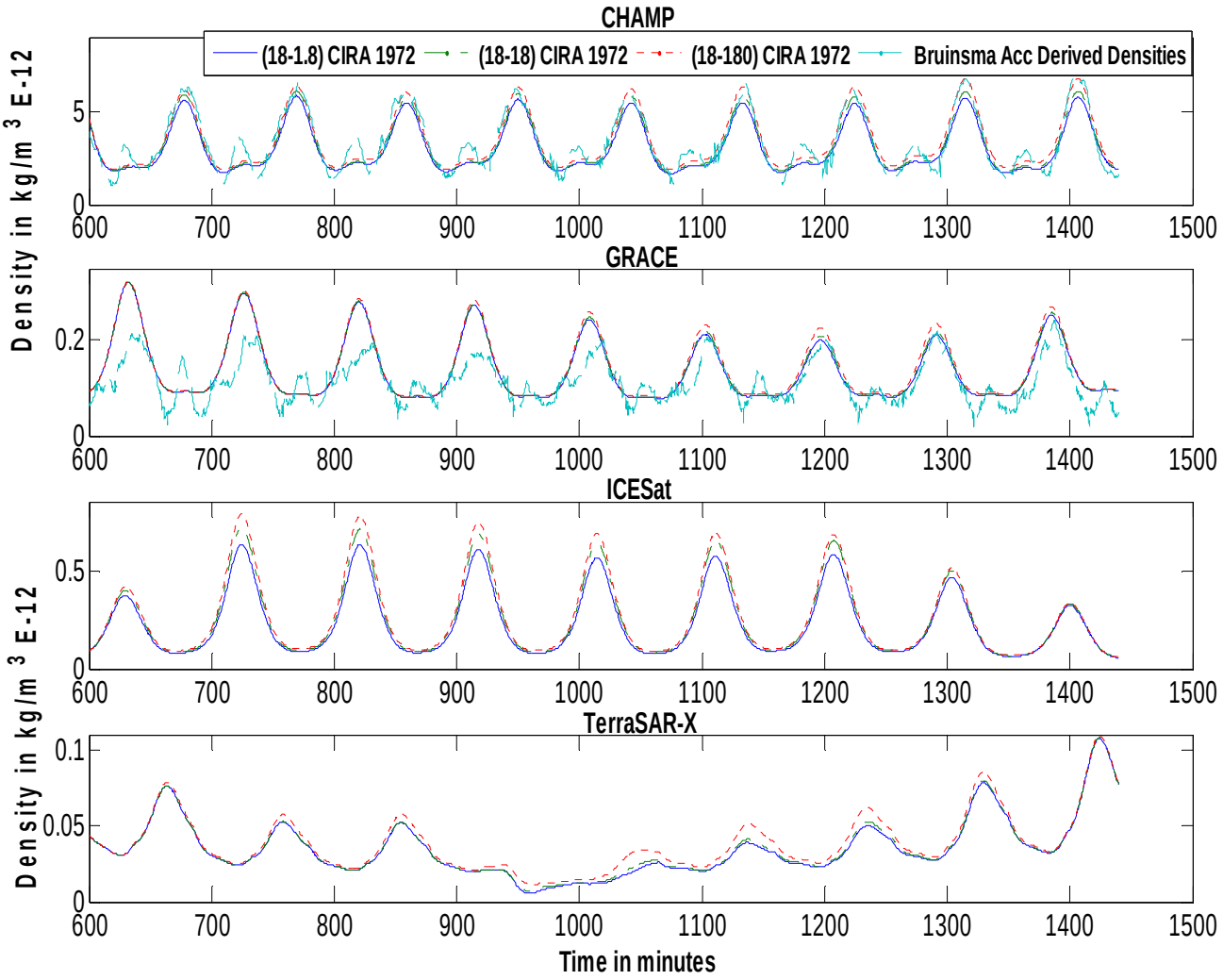

Figure 4.10 **Effect of varying Ballistic Coefficient correlated half-lives on CIRA-72 POE density estimates.**

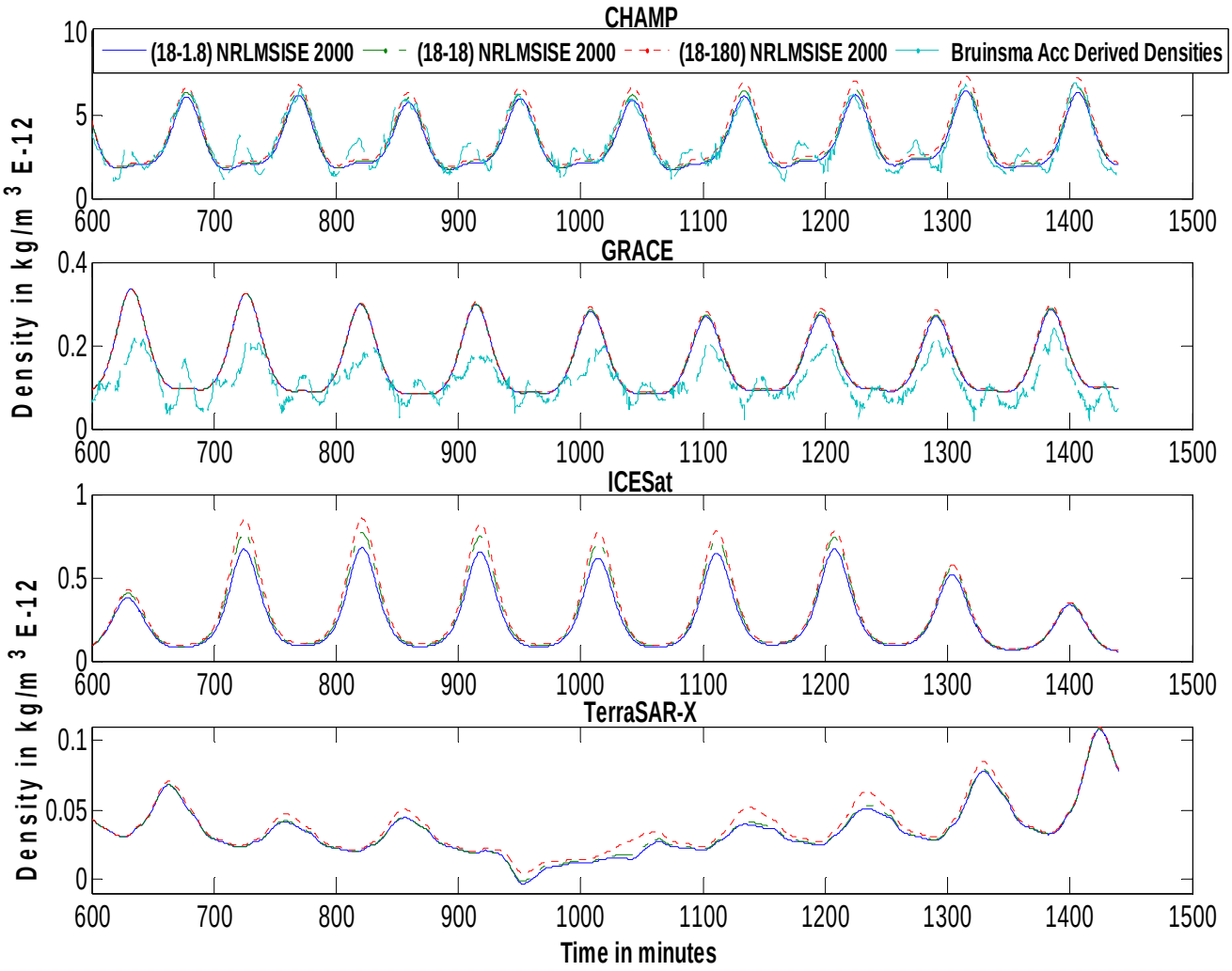

Figure 4.11 **Effect of varying Ballistic Coefficient correlated half-lives on NRLMSISE-00 POE density estimates.**

Figures 4.10 and 4.11 show the variation of POE density estimates with different BC correlated half-lives for Oct 17, 2008. Figures, 4.10 and 4.11 show that the POE density estimates increase with increase in BC correlated half-life. This is opposite to the trend observed in the case of density half-life variation. All four satellites

CHAMP, GRACE, ICESat, and TerraSAR-X, and both the atmospheric density models, CIRA-72 and NRLMSISE-00 exhibit a similar trend in variation of POE density estimates. The accelerometer densities of CHAMP and GRACE correlated better with lower BC correlated half-lives of 1.8 min and 18 min.

4.5 Conclusion

As already mentioned, the main purpose of this chapter is to study the effects of solar activity, geomagnetic activity, density, and BC correlated half-life variation on POE density estimates for the ICESat and TerraSAR-X satellites. Previous research in ref [1], ref [2] showed the effects of these activities on POE density estimates of CHAMP and GRACE. In this chapter the POE density estimates are calculated for more days for all four satellites. The POE density estimates obtained from the CIRA-72 and NRLMSISE-00 atmospheric density models are plotted for each satellite. The trends in the variation of these density estimates for ICESAT and TerraSAR-X are compared to those of CHAMP and GRACE to check the similarity in density variation. For nearly all the cases plotted above the POE density estimates for both ICESat and TerraSAR-X exhibited a similar trend to that of CHAMP and GRACE for NRLSMSISE-00 and CIRA-72 density models. The results obtained for each case of activity is summarized in the following sections.

4.5.1 Solar and Geomagnetic Activity

For all the periods of Solar and Geomagnetic Activity and for all four satellites, the NRLMSISE-00 POE density estimates were higher than CIRA-72 POE density estimates. For CHAMP, GRACE, and TerraSAR-X the Jacchia-71 model densities are higher than NRLMSISE-00 and CIRA-72 POE density estimates. This trend is observed only for low and moderate solar activity, and quiet geomagnetic activity. For active geomagnetic activity, the Jacchia-71 densities were lower than NRLMSISE-00 POE density estimates but higher than CIRA-72 POE density estimates. In the case of elevated and high solar activity, the Jacchia-71 densities were lower than POE density estimates. For CHAMP and GRACE, the CIRA-72 POE density estimates correlated well with the accelerometer densities. Therefore, the POE density estimates generated by correcting the CIRA-72 density model can be considered better than the POE densities generated by correcting the NRLMSISE-00 model.

4.5.2 Density and Ballistic Coefficient Correlated Half-life Variation.

Varying density and ballistic coefficient correlated half-lives resulted in similar variations of POE density estimates for all four satellites. The increase of density correlated half-life resulted in the decrease of POE density estimates. The increase of BC correlated half-life resulted in the increase of POE density estimates. For CHAMP and GRACE the POE densities correlated well with the accelerometer densities for higher density half-lives and lower BC half-lives.

5 SUMMARY, CONCLUSIONS AND FUTURE WORK

5.1 Summary

The atmospheric density varies continuously in the upper atmosphere mainly due to changes in solar and geomagnetic activity. The existing atmospheric density models cannot account for the sudden changes and extreme variations in the atmospheric density. As a result, the density values from these atmospheric models are not accurate enough for calculating the estimates of drag acting on a satellite, which in turn results in an inaccurate prediction of the satellite orbit.

The work done in this research made corrections to existing atmospheric models by using precision orbit ephemerides (POE) data from the ICESat, TerraSAR-X, CHAMP, and GRACE satellites. The POE data obtained from the satellites were run in an orbit determination scheme which performs a sequential filter/smoother to process the measurements and generate corrections to the atmospheric models and estimate density. These densities have greater accuracy over the uncorrected atmospheric model densities and can be used to calculate accurate drag estimates resulting in improved satellite orbit determination.

The validation of corrected atmospheric densities was done by comparing them with accelerometer derived densities for those satellites which have accelerometers on-board. The comparison is done by finding the cross correlation (CC) and root mean square (RMS) values between corrected densities and accelerometer densities. Previous research used the POE data of the Challenging Mini

Satellite Payload (CHAMP) satellite to find the corrected densities. Later, the corrected densities were compared to the accelerometer densities of CHAMP derived by Sean Bruinsma from CNES, Department of Terrestrial and Planetary Geodesy, France. Similar to the Bruinsma densities, we have accelerometer densities derived by Eric Sutton from the University of Colorado. In this research, the consistency of Sutton densities was checked by comparing them with the accelerometer densities derived by Sean Bruinsma.

The consistency of Sutton derived densities was checked for two satellites, CHAMP and the Gravity Recovery and Climate Experiment (GRACE), for different levels of solar and geomagnetic activity. The consistency was checked by finding the CC and RMS values between Sutton derived densities and Bruinsma derived densities. The CC and RMS values were found for several days from the years 2001 to 2007 comprising all different levels of solar and geomagnetic activity. The consistency was also checked by finding the CC and RMS values between POE density estimates, which were obtained as a result of corrections generated to the atmospheric models, and the accelerometer densities derived by Bruinsma and Sutton separately. The comparison was made for the POE densities obtained from the corrections made to all five different atmospheric models, CIRA-72, Jacchia-71, Jacchia-Roberts, MSISE-90, and NRLMSISE-00 using nine different density and ballistic coefficient correlated half-life combinations (1.8-1.8, 1.8-18, 1.8-180, 18-1.8, 18-18, 18-180, 180-1.8, 180-18, 180-180) for both CHAMP and GRACE. The CC

and RMS values thus obtained were tabulated separately for Bruinsma and Sutton and compared to check the consistency between them.

Ice, Cloud and Land Elevation Satellite (ICESat) and Terra Synthetic Aperture Radar X-Band Satellite (TerraSAR- X) were two other satellites analyzed in this research. Unlike the CHAMP and GRACE satellites, ICESat and TerraSAR-X do not possess on-board accelerometers. The main interest in this research work is to check how the POE density estimates of ICESat and TerraSAR-X vary, when compared to the POE density estimates of CHAMP and GRACE. The POE density estimates of all four satellites were obtained by generating corrections to two different atmospheric models, one from the Jacchia model family (CIRA-72) and the other from the Mass Spectrometer Incoherent Scatter (MSIS) model family (NRLMSISE-00). The density values from the Jacchia-71 empirical model were also compared with the corrected POE densities.

A few days from the years 2001 to 2008 were selected and POE density estimates were obtained for those days. These days are classified as low, moderate, elevated, and high solar activity days and quiet, moderate, and active geomagnetic days depending upon their solar flux values and A_p indices. The POE density estimates obtained from each corrected atmospheric model were plotted as curves for all four satellites. The plots for the ICESat and TerraSAR-X satellites were compared with those of CHAMP and GRACE to check how the density estimates vary for each atmospheric model. Comparison was done for different levels of solar and

geomagnetic activity and also by varying density and ballistic coefficient correlated half-lives. All these comparisons helped to determine the trends in the variations of POE density estimates for the ICESat and TerraSAR-X satellites and also to know how these trends differ from those of the CHAMP and GRACE satellites. Since, the actual densities from the empirical Jacchia-71 model are also shown in the plots along with the POE density estimates, the difference among the densities can be observed.

5.2 Conclusions

The following conclusions were made as a result of the work done in this research.

1. For both CHAMP and GRACE satellites, the CC values between Sutton and Bruinsma accelerometer densities ranged between 0.97- 0.98, while the RMS values were around 0.1 – 0.3 kg/m^{3}E-12 for all the selected days from the year 2001 to 2007. This indicates that a good correlation exists between Bruinsma and Sutton densities.

2. The correlation between Bruinsma and Sutton densities slightly worsened during high periods of solar and geomagnetic activity for both CHAMP and GRACE.

3. The correlation between Sutton and Bruinsma densities is higher for GRACE than for CHAMP.

4. The CC and RMS values of the POE density estimates compared to the Bruinsma and Sutton densities are nearly the same. The difference in CC

values was around 0.0001-0.0005, and 0.001–0.003 kg/m^3E-12 for RMS values, which indicates the closeness between Bruinsma and Sutton densities.

5. The Sutton and Bruinsma densities have better correlation with the POE density estimates generated using the Jacchia based models than with those generated using the MSIS based models.

6. The Sutton and Bruinsma densities correlated better with the POE density estimates generated using atmospheric models with higher density half-life and lower ballistic coefficient half-life. The correlations proved to be the best for the density and BC correlated half-life combinations of 18-1.8 min and 180-1.8 min.

7. A similar trend in correlations is observed between the POE density estimates and the Sutton and Bruinsma accelerometer densities for all levels of solar and geomagnetic activity.

8. The accelerometer densities derived by Sutton are nearly identical to the Bruinsma densities. Therefore, Sutton densities can be considered as a substitute for the Bruinsma densities in future work.

9. For the satellites ICESat and TerraSAR-X the POE density estimates generated using the NRLMSISE-00 model are always higher than those generated using the CIRA-72 atmospheric model.

10. CIRA-72 and NRLMSISE-00 POE density estimates are not well correlated with the density values obtained using the Jacchia-71 empirical model for all levels of solar and geomagnetic activity, thus showing the difference between corrected atmospheric model density values and empirical model density values.

11. For ICESat, the Jacchia-71 model densities were always lower than the POE density estimates for all levels of solar and geomagnetic activity. For TerraSAR-X, they were always higher than the POE density estimates for low, quiet, and moderate levels of solar and geomagnetic activity. TerraSAR-X did not experience the days with active, high, and elevated solar and geomagnetic activity during its operational life.

12. An increase in the density half-life for an atmospheric model results in lower POE density estimates, while an increase in BC half-life results in higher POE density estimates.

13. Since the mission life of GRACE and TerraSAR-X do not have days with elevated or high solar and active geomagnetic activity, the behavior of POE density estimates for these satellites for those days cannot be observed.

14. The POE density estimates generated using the CIRA-72 model correlated better than the NRLMSISE-00 POE densities with the accelerometer densities of CHAMP and GRACE.

15. For CHAMP and GRACE, the POE densities correlated better with the accelerometer densities generated using atmospheric models with higher density half-life (180 min) and lower BC half-life (1.8 min).

16. The POE density estimates generated using the CIRA-72 and NRLMSISE-00 atmospheric models for ICESat and TerraSAR-X satellites showed similar trends in variation when compared with those of CHAMP and GRACE for all levels of solar and geomagnetic activity and for all density and BC correlated half-lives.

5.3 Future Work

5.3.1 Considering Sutton Derived Accelerometer Densities

The work conducted in this research showed that the accelerometer derived densities by Sutton are nearly identical to the accelerometer densities derived by Bruinsma for both the CHAMP and GRACE satellites. Therefore, for any further research on CHAMP and GRACE, Sutton's densities can be used as a substitute for Bruinsma densities to validate the POE density estimates generated using atmospheric models.

5.3.2 Examination of POE Density Estimates for ICESat at Low Altitudes

In this research, POE density estimates were obtained for ICESat for many days beginning from its operational life on January 13, 2003 to 2008. After the failure of the last laser on ICESat, it was retired in February 2010 and later decommissioned

on August 14, 2010. Before decommissioning, ICESat was lowered in orbit preparing for orbital decay. The POE data obtained from the GPS onboard the satellite during this period can be used to study the variation of atmospheric density at lower altitudes.

5.3.3 Considering More Satellites and Additional Days

This research focused on CHAMP, GRACE, ICESat, and TerraSAR-X, all of which have different orbits and altitudes. To study more about the variation of atmospheric density, more satellites at different orbits and altitudes are to be considered in future. Satellites such as ANDE (Atmospheric Neutral Density experiment), Jason-1, and Tandem-X have available POE data and can be examined for future work. This research work considered the days only up to year 2008. Especially for ICESat and TerraSAR-X, additional days after 2008 are to be considered for better understanding of the POE density estimates.

5.3.4 Considering Different Density and Ballistic Coefficient Correlated Half-Lives and Atmospheric Models

This research utilized the density and ballistic coefficient correlated half-lives of 1.8 minutes, 18 minutes, and 180 minutes. The POE density estimates generated using these values of half-lives showed wide variation between them. Smaller increments between half-lives results in POE density estimates that could have better correlation with the accelerometer densities. Therefore, future work should consider the usage of half-lives having smaller increments between them to

better understand the POE density estimates. Other than the five atmospheric models used in ODTK, new models such as Jacchia-Bowman 2008 should also be considered for work in future. Using more efficient models can result in more accurate POE density estimates.

REFERENCES

1. Vincent. L. Pisacane, *The Space Environment and its Effects on Space Systems*, AIAA Education Series, Chap. 7
2. D. A. Vallado, *Fundamentals of Astrodynamics and Applications*, Microcosm Press, El Segundo, CA, 3rd Edition, 2007, Chap. 8, App. B.
3. D. Hastings, H. Garrett, *Spacecraft Environment and Interactions*, Cambridge University Press, 1996, Chap 1, 3, and 4.
4. A. C. Tribble, *The Space Environment: Implications for Spacecraft Design*, Princeton University Press, Princeton, New Jersey, 2003.
5. D. King-Hele, *Satellite Orbits in an Atmosphere*, Springer, 1st Edition, 1987, Chap 1&2.
6. D. A. Vallado, D. Finkleman, "A Critical Assessment of Satellite Drag and Atmospheric Density Modeling", AIAA 2008-6438, AIAA/AAS Astrodynamics Specialist Conference, Honolulu, Hi, 2008.
7. National Geophysical Data Center, *Solar Indices Bulletin*, Boulder, CO: National Geophysical Data Center, http://www.ngdc.noaa.gov/ and ftp://ftp.ngdc.noaa.gov/STP/SOLAR_DATA/SOLAR_RADIO/FLUX.
8. National Geophysical Data Center, *Solar Indices Bulletin*, Boulder, CO: National Geophysical Data Center, http://www.ngdc.noaa.gov/ and ftp://ftp.ngdc.noaa.gov/STP/GEOMAGNETIC_DATA/INDICES/KP_AP/.
9. L. G. Jacchia, *Revised Static Models for the Thermosphere and Exosphere with Empirical Temperature Profiles*, SAO Special Report No. 332, Smithsonian Institution Astrophysical Observatory, Cambridge, MA, 1971.
10. C. E. Roberts, Jr., "An Analytic Model for Upper Atmosphere Densities Based upon Jacchia's 1970 Models," *Celestial Mechanics*, Vol. 4, Issue 3-4, December 1971, pp. 368-377.
11. COSPAR Working Group IV, *COSPAR International Reference Atmosphere*, Akademie-Verlag, Berlin, 1972.
12. A. E. Hedin, "Extension of the MSIS Thermosphere Model into the Middle and Lower Atmosphere," *Journal of Geophysical Research*, Vol. 96, 1991, pp. 1159-1172.
13. J.M. Picone, A. E. Hedin, D. P. Drob, "NRLMSISE-00 Empirical Model of the Atmosphere: Statistical Comparisons and Scientific Issues," *Journal of Geophysical Research*, Vol. 107, No. A12, 2002.
14. V. S. Yurasov, A. I. Nazarenko, P. J. Cefola, and K. T. Alfriend, "Results and Issues of Atmospheric Density Correction," *Journal of the Astronautical Sciences*, Vol. 52, No. 3, July-September 2004, pp. 281-300.
15. P. J. Cefola, R. J. Proulx, A. I. Nazarenko, and V. S. Yurasov, "Atmospheric Density Correction Using Two Line Element Sets as the Observation Data," *Advances in the Astronautical Sciences*, Vol. 116, AAS 03-626, Univelt, 2003, pp. 1953-1978.

16. M. F. Storz, B. R. Bowman, Major J. I. Branson, S. J. Casali, and W. K. Tobiska, "High Accuracy Satellite Drag Model (HASDM)," *Advances in Space Research*, Vol. 36, Issue 12, 2005, pp. 2497-2505.
17. Sabol C. A, Kim Lu. K, "Atmospheric Density Dynamics and Motion of the Satellites", *AMOS Technical Conference*, Hi, 2002.
18. C. A. McLaughlin and B. S. Bieber, "Neutral Density Determined from CHAMP Precision Orbits," *Advances in the Astronautical Sciences*, Vol. 129, AAS 07-260, Univelt, 2008, pp. 167-186.
19. S. Bruinsma and R. Biancale, "Total Densities Derived from Accelerometer Data," *Journal of Spacecraft and Rockets*, Vol. 40, No. 2, March-April 2003, pp. 230-236.
20. A. Hiatt, "Deriving Atmospheric Density Estimates Using Satellite Precision Orbit Ephemerides," M.S. Thesis, University of Kansas, 2009.
21. T. Lechtenberg, "Derivation and Observability of Upper Atmospheric Density Variations Utilizing Precision Orbit Ephemerides," M.S. Thesis, University of Kansas, 2010.
22. J. van den Ijssel, P. Visser, and R. Haagmans, "Determination of Non-Conservative Accelerations from Orbit Analysis," *Earth Observation with CHAMP Results from Three Years in Orbit*, eds. C. Reigber, H. Luhr, P. Schwintzer, J. Wickert, Springer, Berlin, 2005, pp. 95-100.
23. J. van den IJssel and P. Visser, "Performance of GPS Accelerometry: CHAMP and GRACE," *Advances in Space Research*, Vol. 39, 2007, pp. 1597-1603.
24. J. van den IJssel and P. Visser, "Determination of Non-Gravitational Accelerations from GPS Satellite-to-Satellite Tracking of CHAMP," *Advances in Space Research*, Vol. 36, 2005, pp. 418-423.
25. C. A. McLaughlin, A. Hiatt, and T. Lechtenberg, "Precision Orbit Derived Total Density", Vol. 48, No. 1, *Journal of Spacecrafts and Rockets*, February 2011.
26. A. Hiatt, C. A. McLaughlin, and T. Lechtenberg, "Deriving Density Estimates Using CHAMP Precision Orbit Data for Periods of High Solar Activity," *Advances in the Astronautical Sciences*, Vol. 134, AAS 09-104, Univelt, 2009, pp. 23-42.
27. NASA, Goddard Space Flight Centre, "ICESAT", Last Accessed: March 30, 2011, http://icesat.gsfc.nasa.gov/icesat/
28. EADS, Astrium, "TerrSAR-X", http://www.infoterra.de/terrasar-x-satellite, Last Accessed: March 30, 2011.
29. GFZ German Research Centre for Geosciences, "CHAMP", Last Accessed: March 30, 2011, http://op.gfz-potsdam.de/champ/main_CHAMP.html.
30. GFZ German Research Centre for Geosciences, "GRACE", Last Accessed: March 30, 2011, http://www.gfz-potsdam.de/portal/gfz/projects/grace
31. B. D. Tapley, B. E. Schutz, and G. H. Born, *Statistical Orbit Determination*, Elsevier Academic Press, Amsterdam, 2004.

32. O. Montenbruck and E. Gill, *Satellite Orbits: Models, Methods, and Applications*, Springer-Verlag, Berlin, 2001.
33. J. R. Wright, "Optimal Orbit Determination," *Advances in the Astronautical Sciences*, Vol. 112, AAS 02-192, Univelt, 2002, pp. 1123-1134, http://www.agi.com/downloads/support/productSupport/literature/pdfs/whitePapers/optimal_od.pdf.
34. A. Milani, G. Gronchi, *Theory of Orbit Determination*, Cambridge University Press, 1st Edition, 2009.
35. J. R. Wright, "Real-Time Estimation of Local Atmospheric Density," *Advances in the Astronautical Sciences*, Vol. 114, AAS 03-164, Univelt, 2003, pp. 927-950.
36. J. R. Wright and J. Woodburn, "Simultaneous Real-Time Estimation of Atmospheric Density and Ballistic Coefficient," *Advances in the Astronautical Sciences*, Vol. 119, AAS 04-175, Univelt, 2004, pp. 1155-1184.
37. Analytical Graphics, Inc., "Orbit Determination Tool Kit Help," *Orbit Determination Tool Kit*, Version 5.1.3.
38. J. R. Wright, "Orbit Determination Tool Kit Theorems and Algorithms," *Analytical Graphics, Inc.*, 2007.
39. G. Welch, G. Bishop, "An Introduction to the Kalman Filter", University of North Carolina- Chapel Hill, TR 95-041, July 2006, http://www.cs.unc.edu/~welch/media/pdf/kalman_intro.pdf , Last accessed: March 30, 2011.
40. R. S. Hujsak, J. W. Woodburn, John H. Seago, "The Orbit Determination Tool Kit (ODTK) - Version 5", *Advances in the Astronautical Sciences*, Vol. 127, AAS 07-125, Univelt, 2007, pp. 381-400.
41. Interpolation of Tabular Data with Cubic Splines, http://www.cdeagle.com/nanum/demosfit.pdf, Last accessed: March 30, 2011
42. D. A. Vallado, T. S. Kelso, "Using EOP and Space Weather Data For Satellite Operations", *Advances in the Astronautical Sciences*, AAS 05-406, Astrodynamics Specialist Conference, CA, 2005, pp. 2473-2492.
43. J. Woodburn, S. Lynch, "A Numerical Study of Orbit Lifetime", *Advances in the Astronautical Sciences*, Vol. 123, AAS 05-297, Univelt, 2005, pp. 789-803.
44. S. Tanygin and J. R. Wright, "Removal of Arbitrary Discontinuities in Atmospheric Density Modeling," *Advances in the Astronautical Sciences*, Vol. 119 II, AAS 04-176, Univelt, 2004, pp. 1185-1196.
45. Z. J. Folcik, "Orbit Determination Using Modern Filters/Smoothers and Continuous Thrust Modeling", MS thesis, MIT, 2008.
46. P. Bourke, "Cross Correlation," August 1996, Last Accessed: March 30, 2011, http://local.wasp.uwa.edu.au/~pbourke/miscellaneous/correlate/.
47. S. Bruinsma, S. D. Tamagnan and R. Biancale, "Atmospheric Densities Derived from CHAMP/STAR Accelerometer Observations," *Planetary and Space Science*, Vol. 52, 2004, pp. 297-312.

48. R. S. Nerem, J. M. Forbes, E. K. Sutton, and S. Bruinsma, “Atmospheric Density Measurements Derived from CHAMP/STAR Accelerometer Data,” *Advances in the Astronautical Sciences*, Vol. 116, AAS 03-621, Univelt, 2003, pp. 1879-1898.
49. E. D Fattig, C. A McLaughlin, “Comparison of Density Estimation for CHAMP and GRACE Satellites”, AIAA 2010-7976, *2010 AIAA Guidance, Navigation and Control Conference*, Toronto, Ontario, Canada, August 2010.